UNIVERSITA' DEGLI STUDI DI VERONA

DEPARTMENT OF NEUROLOGICAL, NEUROPSYCHOLOGICAL,
MORPHOLOGICAL AND MOVEMENT SCIENCES

GRADUATE SCHOOL OF
SCIENCES ENGINEERING MEDICINE

DOCTORAL PROGRAM IN
MULTIMODAL IMAGING IN BIOMEDICINE

Cycle 25 / 2010

Three-dimensional body scanning: methods and applications for anthropometry

S.S.D. Bio/16

Coordinator: Prof. Andrea Sbarbati

Tutor: Prof. Carlo Zancanaro

Doctoral Student: Dott. Christian Lovato

Credits

Thanks to my many fellows for help all the intriguing conversations, in particular to Riccardo Gherardi, for his suggestions about the first implementation of APT.

Most of this work couldn't have been performed without the precious contribute of prof. Andrea Giachetti, Department of Informatics, University of Verona.

Table of Contents

Abstract

In this thesis we describe the developed computer method and experiments performed in order to apply whole body 3D scanner technology in support to anthropometry. The output of whole body scanners is a cloud of points, usually transformed in a triangulated mesh through the use of specific algorithms in order to support the 3D visualization of the surface and the extraction of meaningful anthropometric landmarks and measurements. Digital anthropometry has been already used in various studies to assess important health-related parameters.

Digital anthropometric analysis is usually performed using device-specific and closed software solutions provided by scanner manufacturers, and requires often a careful acquisition, with strong constraints on subject pose. This may create problems in comparing data acquired in different places and performing large-scale multi-centric studies as well as in applying advanced shape analysis tools on the captured models.

The aim of our work is to overcome these problems by selecting and customizing geometrical processing tools able to create an open and device-independent method for the analysis of body scanner data. We also developed and validated methods to extract automatically feature points, body segments and relevant measurements that can be used in anthropometric and metabolic research.

In particular we present three experiments. In the first, using specific digital anthropometry software, we evaluated the Breuckmann BodySCAN for performance in anthropometric measurement. Subjects of the experiment were 12 young adults underwent both manual and 3D digital anthropometry (25 measurements) wearing close-fitting underwear. Duplicated

manual measurement taken by one experienced anthropometrist showed correlation r 0.975-0.999; their means were significantly different in four out of 25 measurements by Student's t test. Duplicate digital measurements taken by one experienced anthropometrist and two naïve anthropometrists showed individual correlation coefficients r ranging 0.975-0.999 and means were significantly different in one out of 25 measurements. Most measurements taken by the experienced anthropometrist in the manual and digital mode showed significant correlation (intraclass correlation coefficient ranging 0.855-0.995, $p<0.0001$). We conclude that the Breuckmann BodyScan is reliable and effective tool for digital anthropometry.

In a second experiment, we compare easily detectable geometrical features obtained from 3D scans of female obese (BMI > 30) subjects with body composition (measured with a DXA device) of the same subjects, in order to investigate which measurements on shape descriptors better correlate with torso and body fat. The results obtained show that some of the tested geometrical parameters have a relevant correlation, while other ones do not strongly correlate with body fat. These results support the role of digital anthropometry in investigating health-related physical characteristics and encourage the realization of further studies analyzing the relationships between shape descriptors and body composition.

Finally, we present a novel method to characterize 3D surfaces through the computation of a function called Area Projection Transform, measuring the likelihood of points in the 3D space to be center of radial symmetry at selected scales (radii). The transform can be used to detect and characterize robustly salient regions (approximately spherical and cylindrical parts) and it is, therefore, suitable for applications like anatomical features detection. In particular, we show that it is possible to build graphs joining these points following maximal values of the MAPT (Radial Symmetry Graphs) and that these graphs can be used to extract relevant shape

properties or to establish point correspondences on models robustly against holes, topological noise and articulated deformations.

It is concluded that whole body scanning technology application to anthropometry are potentially countless, limited only by the ability of science to connect the biological phenomenon with the appropriate mathematical/geometrical descriptions.

Most of the present thesis comes from the following papers:

- Andrea Giachetti, Christian Lovato, *Radial Symmetry Detection and Shape Characterization with the Multiscale Area Projection Transform* «COMPUTER GRAPHICS FORUM» , vol. 31 , n. 5 , 2012 , pp. 1669-1678
- C. Lovato, C. Milanese, F. Piscitelli, C. Zancanaro, A. Giachetti, *Health-related shape analysis of 3D body scanner data* in Proceedings 2nd International Conference on 3D Body Scanning Technologies a cura di N. D'Apuzzo , Atti di "2nd International Conference on 3D Body Scanning Technologies" , Lugano, Switzerland , 25-26 October 2011 , 2011 , pp. 87-94
- Lovato C.; Milanese C.; Giachetti A.; Zancanaro C., *3D digitral anthropometry using the bodySCAN* in Proceedings of the International Conference on 3D body Scanning Technologies , Hometrica Consulting - Switzerland , Atti di "3D body scanning technologies" , Lugano , 19-20 ottobre 2010 , 2010 , pp. 255-259
- Christian Lovato, Umberto Castellani, Simone Fantoni, Chiara Milanese, Carlo Zancanaro, Andrea Giachetti, Computer assisted estimation of anthropometric parameters from whole body scanner data in N. Magnenat-Thalmann (Ed.): 3DPH 2009 a cura di N. Magnenat-Thalmann , Springer, Heidelberg , Atti di "Workshop on 3D Physiological Human (3DPH) 2009" , Zermatt , 29/11-2/12/2009 , 2009 , pp. 71-83

1. Introduction

Anthropometry has been used for decades in physical anthropology to measure individual human beings in order to quantify human physical variations; moreover, it is currently utilized in several biological and medical settings in order to obtain population reference data, carry out health surveys, perform nutritional assessment and so on. Further, anthropometry is of use in forensic medicine to identify individuals, ergonomics to produce best-fitting objects and tools as well as the clothing industry to realize optimized garment.

Along the last 150 years, anthropometry has been manually performed by trained personnel using dedicated instruments such as tapes, calipers of different sizes and shapes, stadiometers, etc [1]; an advantage of manual anthropometry is that it is relatively cheap and can be performed in- and outdoors with minimal effort; drawbacks are, among others, that inter- and intra-observer variability in measurement may be fairly large (hence the need for trained personnel) [2,3] and the information obtained is limited to actual measurements, because the subject must be physically present to allow any measurement.

More recently, 3D scanning technology has come of age to enable anthropometry in an entirely new way (see e.g. [4]). Nowadays, a number of 3D scanners are available on the market, which can be adapted to anthropometric measurements; these devices are usually developed using laser or Moiré-fringing-based technologies. In the former a laser stripe is projected onto the body surface and several cameras acquire images: in this way 3D points representing the body shape can be recovered by triangulation. Examples of this kind are the scanners developed by Cyberware [5], Hamamatsu [6], Vitronic [7] or Human Solutions [8]. In the latter, one or more projectors create light patterns on the body surface and 3D points are

estimated by observing the pattern deformations on the body surface with a set of cameras. Examples of this kind are the scanners developed by Textile and Clothing Technology Corporation [9], Telmat [10] inSpeck [11], and the product used for our experiments, i.e. the BodySCAN developed by Breuckmann GmbH [12].

This research is focused on the application of modern 3D shape analysis techniques to the measurement of body shape (as acquired through body scanner) in order to obtain useful information related to the health of the measured subjects. In particular we investigated the ability of digital measurements to predict body fat, because fat is involved in important health related issues, besides to be usually connected with visible changes in body shape. Moreover, computer techniques and tools developed by our team for mesh analysis is described.

We start this chapter introducing some basic notions on anthropometry and mesh analysis. After, we introduce our experiments with the body scanner e.g. one describing the validation of our body scanner and a second where connection of digital measurement with body fat is investigated . We report also a computer technique that has been developed by our group for body shape analysis. In the second chapter the methods of the experiments are described. In chapter 3 the main results of presented research are reported. Obtained results are discussed in chapter 4. For clarity, in Figure 1 we show a diagram where the methods and experiments presented in the thesis are summarized.

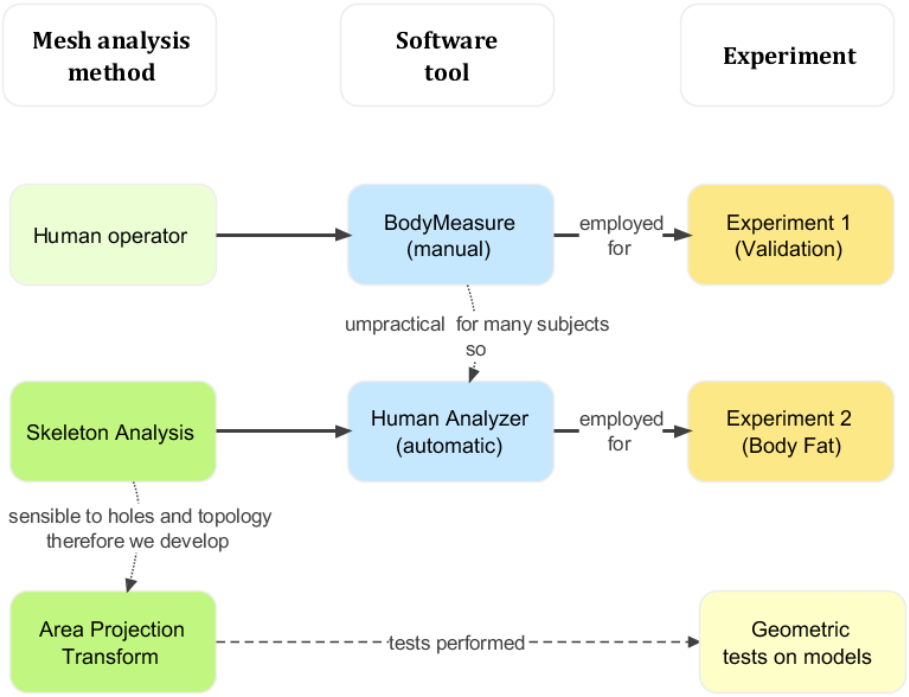

Figure 1: we developed two software tools that allow derive anthropometric measurements from scanner data. Those data are complex, so a method for analyze them is mandatory. In the manual tool, the agent that analyzes them is the human operator, while in the automatic one we use curve skeleton analysis for the purpose. We report two anthropometric experiments each using one of the tools. We further developed a new method and reported the experiments we performed to investigate its suitability for mesh analysis.

Body fat and anthropometry

Information about body size and shape has traditionally been used by physicians to assess health or nutritional status and guide treatment. More recently, anthropometric indices have been used to classify normal weight, overweight, and obese individuals as well as to identify individuals at increased risk of e.g., myocardial infarction. Obesity is has been demonstrated to be a risk factor for the metabolic syndrome [13, 14], cancer [15] and poor lung function [16].

Interestingly, visceral adipose tissue is most strongly associated with dyslipidaemia, dysglycaemia, and indices of cardiovascular disease. Good correlation between visceral fat and waist circumference has been repeatedly shown, although several systematic bias are

apparent with that measurement; an association between body (visceral) fat and insulin resistance, a key factor in type II diabetes and the elusive syndrome X is also present. On the contrary, thigh circumference has been shown to be protective for both heart disease and type II diabetes mellitus.

While the gold standard for the assessment of body fat are underwater weight measurement and, more recently, DXA exam, several authors [17] studies the application anthropometric analysis through body scanner for this aim.

Automatic Measurements

Body scanning allows to perform a big number of acquisitions in relatively few time. Has become desirable for anthropometrists use software tools that automatically process the data and perform automatic measurements.

Methods to extract anthropometric features in an interactive or automatic way have been proposed by several authors. In [18] methods for computer assisted estimation of values used in the garment industry are presented. 3D scanners are in some cases provided with software tools able to extract automatic or semi-automatic sets of measurements. A comparison of data provided by some of these tools, showing capabilities but also limitations and inconsistencies is presented in [19]. In the CAESAR project, Robinette et al. [4] developed a semi-automatic method to locate landmarks based on the placement of markers on the scanned body and the user assisted location of markers on scanner images. Landmarks are then labeled and used for the measurement estimation. Ben Azouz et al. [20] developed a method to locate automatically, using features known as spin images, the landmarks used in the CAESAR project and validated the results with manual placement).

Results, however, due to the intrinsic complexity of the problem (many features are located manually by palpation), are not always accurate. Leong et al [21] computed automatically a set of 21 landmarks and 35 feature lines from scanner data, with a method based on the processing of depth maps (and therefore pose dependent). Automatic measurements require a refined processing of body scanner data, so we will next introduce some notions about the way scanner data are structured how can be manipulated and analyzed.

Mesh processing

The output of a 3D scanner is a numeric representation of a surface. The scanner reconstruct the acquired surface of the physical body in a digital form that is composed by a big number of triangles (from some tens of thousands to a million depending on the desired resolution) positioned in the 3D space. The union of those 3D digital triangles is called triangular mesh or, simply, mesh. In Figure 2 is shown an example of a mesh generated by the scanner. A detail of the mesh is magnified to show the composing triangles.

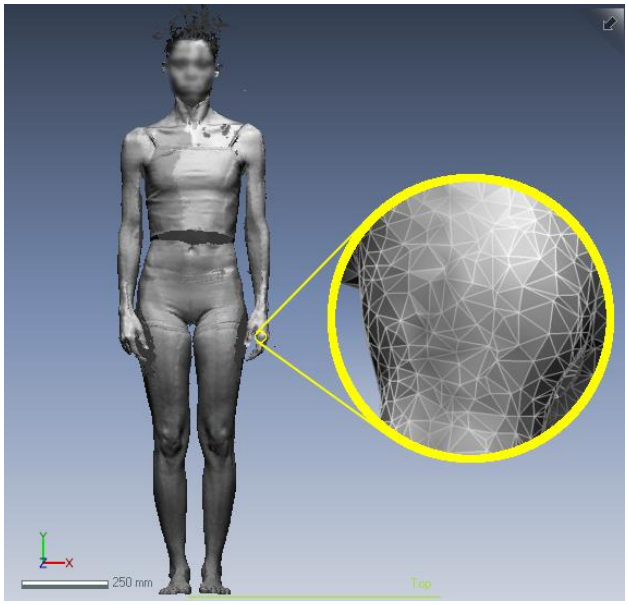

Figure 2: Mesh example, a particular has been magnified and edges enhanced in order to show triangles

Mesh processing is the science of the designing design efficient algorithms for the analysis, elaboration and transmission of digital 3D surfaces. It's a fast growing field of computer graphics whose importance has been improved by diffusion of relatively cheap scanners. Mesh processing techniques uses special data structures to maintain information and requires special mathematical applications (i.e. topology and differential geometry applied to surfaces). Research on this field is strongly applied in multimedia, biomedical (especially imaging) and scientific computing. Most of the algorithms adopted in this research pertain to this field.

Mesh Segmentation

One of the most important area of mesh processing research is mesh segmentation, that study those algorithms devoted to distinguish different subparts in a given 3D mesh or shape. This subdivision can be conducted through several criteria, that can be purely geometrical or (in more recent development) try to be semantic, i.e. distinguish features that is relevant in the context of the specific shape. A huge literature is available on mesh segmentation. However, not so many paper deal with the reliable partitioning of a human body model into semantically consistent parts. A recent detailed review on scanned human body processing methods [22], presents and compare only few methods applied in literature to perform this task, most of them limited to standard postures, except for those based on Reeb Graphs [23,24]. Mortara et al. [25] proposed the use of a surface point classification called plumber in order to identify tubular region and extract body parts, performing also anthropometric measurements. Yu et al. [26] proposed a method able to find automatically joints by computing specific measurements on volume sections. The method, however, requires a previous detection of body landmarks and limbs direction.

Salient point detection

Another way we can use to analyze meshes is through the automatic identification of salient points, that are points that possess specific properties in the context of the shape. The notion of salient point in computer graphics is operatively equivalent to that of "anatomical landmark" in anthropometry. Several approaches have been proposed to detect and describe salient points or geometrical location characterizing 3D shapes. Most of them are designed to find surface features through curvature analysis at different scales and to describe them with feature vectors depending on the local neighborhood. A curvature-base notion of mesh saliency has been proposed in [27] and many papers presented related methods to detect and describe salient points on surfaces [28,29]. Shape descriptors can be purely local [30, 31] or add global information to obtain a more reliable point characterization [32]. Local and global descriptors can then be used for shape retrieval applications with approaches like bag of features or similar ones [33, 34].

Curve skeleton analysis

A popular method to characterize salient locations of 3D shapes is using the 1D curve skeleton [35], a subset of the medial axis [36]. Examples of 3D curve skeletons are shown in Figure 3. Curve skeleton analysis of shape has been introduced for analysis of 2D objects represented in images and subsequently extended in the field of 3D. Briefly speaking, skeleton analysis try to interpret the shape as sustained by a geometrical curve (like the anatomical skeleton) that approximate the centerline in those parts of the shape where is possible to individuate it. Thanks to its 1D structure, curve skeleton captures well the tree-like structure of many real objects and has been used widely used in shape recognition and matching tasks [37]. The curve skeleton, however, is not well defined where the shape is not approximately tubular and

different algorithms used to compute it give different results and are often sensitive to noise and topological changes.

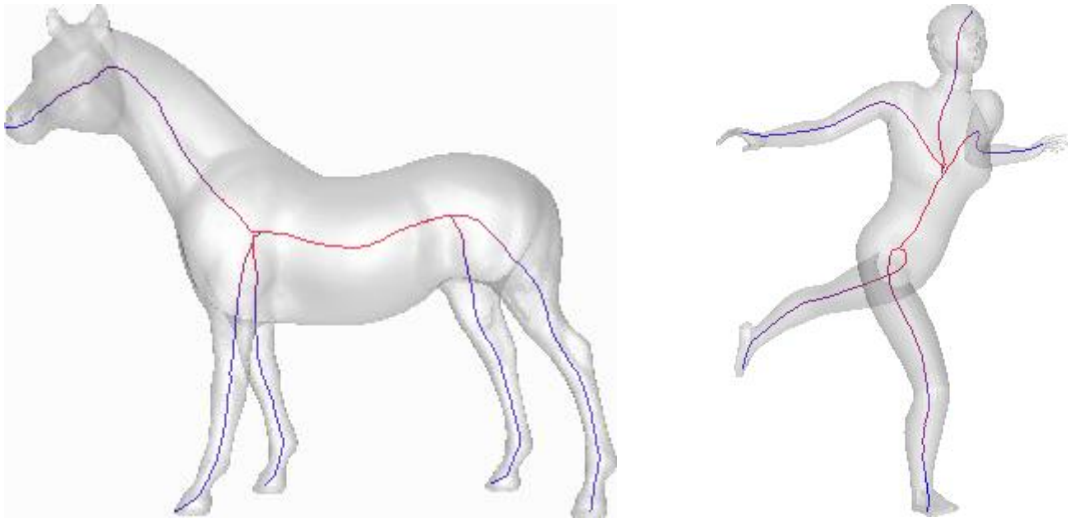

Figure 3: Examples of curve skeletons of 3D shapes

The literature on curve skeleton extraction is also huge and research on this topic is still active. Despite its apparent simplicity, in fact, the extraction of a 1D connected curve skeleton from volume data presents several problems, and even the definition of a curve skeleton is not easy, as pointed out by Cornea et al. [38].

The first methods successfully applied were those based on topological thinning [39], i.e. the iterative removal of external voxels preserving the topology or on the computation of distance maps from the border as in the voxel coding method [40]. They gave useful results, especially in the medical field, where the estimation of a centerline path in vessels is fundamental their characterization and measurement. These techniques, however, usually required interaction to place seed points or extremal points of the skeleton to be preserved. Furthermore results obtained were usually not reliable for non-tubular objects.

A variety of approaches has then been proposed to overcome these problems. Telea and van Wijk [41] used the intersection of 2d skeletons for a fast 3D skeleton extraction, Cornea et al. [42] used a fast marching method, Sharf et al. [43] obtained the skeleton "on the fly" while reconstructing the mesh with a surface growth. Shapira et al. [40] used a function defined on the surface (Shape Diameter Function) in order to find approximate skeletal points then fitted into curves. Dey and Sun [44] removed ambiguities in curve-skeleton definition by considering it as the subset of the medial axis where a function called Medial Geodesic Function can be defined and is singular. A similar approach, but defined on voxelized volumes has been used by Reniers et al. [45]. Drawbacks of these approaches are the complexity of the discretization steps and the computational weight of the geodesic path evaluation.

Aims

We had three main research aims. The first is the validation of the Breuckmann Body Scanner, the whole body scanner device that has been used for my research. The second aim is the investigation of ability of full-automatic anthropometric digital measurements to correlate with relevant health related parameters. The third aim is the development of a robust method for mesh analysis. Each aim was pursued with distinct experiments labeled Experiment 1, Experiment 2, and Experiment 3.

Experiment 1

Validation of the Breuckmann BodyScan for anthropometry

Traditional anthropometry, performed with tape and calipers, is time consuming and is prone to measurement errors when performed by less than higher trained personnel; moreover it

can be uncomfortable for measured subjects that are usually undressed during the measurement [17]. On the other hand, over the last several years, while 3D whole-body scanners spread, a number of three-dimensional (3D) anthropometric studies have been performed using fast and contact free measurements obtained by those devices. Examples are Caesar project [4], SizeUK [46] and SizeUSA [47].

The first goal we pursue is to evaluate the reliability of Breuckmann BodyScan for anthropometry, comparing its performance with measurements obtained through traditional manual anthropometry.

Experiment 2

Health-related shape analysis of 3D Scanner Data

In the second aim presented in this thesis, we test the ability of body scanner to execute automatic measurements correlated with important physiological parameters relating the body fat. Body shape measurements (e.g. W/H ratio) can be used as an indirect assessment of fat content and distribution and are known to correlate with the risks of developing certain diseases, e.g. the metabolic syndrome and diabetes. 3D scanners are able to provide complete digital models of the subjects bodies, encoding a huge amount of information that can be processed automatically making it easier for physicians to evaluate compact descriptors that can be correlated with body composition or diagnostic variables.

From the digital models, in fact, it is possible to extract not only a wide set of measurements usually picked up from manual anthropometry, but also, using geometry processing techniques, to derive parameters related to curvatures, statistical variations of local and global

properties, salient points location, etc. that may well capture most relevant shape variations in the analyzed population.

It may be difficult, however, to compare manual anthropometric measurements and parameters computed on digital models, because the first ones are based on the identification of anatomical landmarks, obtained through observation and palpation by expert anthropometrists which are difficult to be located only on the basis of marker-less digital acquisitions.

For this reason we decided not to compare directly manual anthropometry with digital evaluation of geometrical parameters, but we focused our investigation on measurements that are objective and easily (or automatically) computed from optical scanner data to see if they correlates with composition data to a comparable (or better) extent of traditional measurements.

For the measurement has been employed an automatic tool we developed (briefly described in Methods) device independent able to process raw body scanner data performing re-meshing, body segmentation and skeletonization that provides automatically a set of geometrical descriptors of the torso region. We computed this set of parameters on 3D models of obese female subjects that also underwent traditional anthropometric procedures and dual-energy X-ray absorptiometry (DXA).

To investigate the medical interest of shape related parameters, we evaluated the ability of the computed descriptors and of a set of traditional anthropometric measurements (e.g. selected diameters and lengths), to predict total body fat or trunk fat (as measured by DXA) by means of linear regression analysis. The use of 3D body scanners for studying obesity is not entirely new; several scanner manufacturers provide software tools to collect sets of measurements that can be used to analyze body shape, and these anthropometric data have

been recently correlated with metabolic parameters in validation studies [48,49,50]. A relevant drawback of these tools is that they are not standardized: parameters often are strongly dependent on the acquisition device, and on pose [19], and there are not advanced tool to extract all the relevant medical information from the whole geometry.

The novelty of our approach is that we aim at working out a new measurement procedure using parameters that could be easily obtained from on any sufficiently accurate 3D model, possibly with few pose requirements. The software tool and the experimental study here described are designed as first steps in the development of an open system for the analysis of body shape features related to obesity and other diseases. Material and methods, results and discussion of this research are described in the equivalent chapter of the thesis.

Experiment 3

Development of a new technique for mesh analysis

During the advancement of this research, it has become clear that the tested method for mesh analysis weren't able to cope with some specific issues of our body scanner data. We found two main problems that make our acquired meshes far from ideal. The first is the problem of holes, shared by all body scanners, derived from the lack of data where parts of the body are out of the optics (camera and/or projector) sight.

The second problem derives from the fact that, if pose changes, the topology of the acquired mesh can change consequently and so assume different conformations. For example, while the curve skeleton of a subject in standard anthropometric position is analogue to a center with five extremities (head plus four limbs), if we acquire a subject with joint palms the skeleton become analogue to a center with three extremities (head and legs) plus a ring formed by the

two arms. Those changes in topology can disturb algorithms of pose detection that use topology to find discriminate the limbs. Algorithms that are based on geodesic distance (like HKS) are similarly troubled by this kind of problems that practically limit the variability of subject poses that is suitable for automatic measurement. Finally, the disposition and dimension of holes varies as the pose of subject changes, making hole-filling algorithms less useful than in fixed-pose anthropometric analysis.

Those considerations made us put effort in the development of a new algorithm for mesh analysis whose premises are good in order to obtain robustness against the presence of holes and variability in pose. The algorithm, named Area Projection Transform, is presented in Methods and preliminary experiments are shown in Results.

2. Materials and Methods

Most of the operations performed in this research have been realized through customized computer tools. We developed those tools on the basis of the data produced by BodyScan, but they are suitable for the processing and analysis of most of 3D superficial data obtained by other analogue devices. In this sense, these are general tools for anthropometric analysis of body scanner data.

Breuckmann BodySCAN

The Breuckmann BodySCAN uses high-speed cameras and a proprietary algorithm to detect the actual position of visible light points projected onto the surface of the body through diffraction fringes and reflected to the cameras. Breuckmann BodySCAN typical acquisition consists of about 400.000 points with a precision from 0.2 mm to 1.4 mm, with a time acquisition of 2.5 or 5.5 seconds, depending on the acquisition mode. In our experiments we found that this acquisition time is enough to obtain sufficient quality for the subsequent processing. The scanner output consists of a triangular mesh obtained by the registration and merging of the points acquired by the different cameras. Meshes are, however, not very clean, presenting various types of defects like holes, non-manifold edges, bad shaped triangles and outliers, so a pre-processing step is mandatory. Meshes nodes include also grayscale information. This is extremely important in order, for example, to acquire landmarks position useful for automatic or computer assisted measurements by exploiting natural or added texture (i.e. skin markers).

Figure 4 shows the acquisition setup. Subjects are usually scanned standing in the anatomical position, nevertheless is possible to change the position in order to obtain a better view of specific body parts or analyze different situations, e.g. muscle contraction.

Figure 4: The Breuckmann BodySCAN during acquisition

Experiment 1

Validation of the Breuckmann BodyScan

We describe the methods of the first experiment. Results and discussion of the same are in the corresponding chapters.

Subjects

Six men and six women, students at the University of Verona, were enrolled in this study after informed consent; the study protocol was in accordance to the Helsinki declaration. The main physical characteristics of the study group were as follows: mean age 22,7±2,16 years (range:

20-27); mean height 168,2±7,38 cm (range: 159-184); body mass 61,5±6,16 kg (range: 53-70). Body mass was assessed to the nearest 0.1 kg using a certified electronic scale (Tanita electronic scale BWB-800 MA (Wunder SA.BI. Srl)). Height to the nearest 0.01 m was measured using a Harpenden portable stadiometer (Holtain Ltd., Crymych, Pembs. UK). During scanning and anthropometry, subjects wore close-fitting underwear.

BodyMeasure, a tool for digital anthropometry

In order to perform anthropometric measurements on the models acquired through the body scanner, a virtual tool has been employed that allows anthropometrists to perform body measurements similar to those performed in classical anthropometric procedures. The virtual tool furnishes the digital analogues of tape and calipers. The tool has been developed in a previous collaboration with prof. Zancanaro.

The measurement tool consists of a user friendly interface (see Figure 5) developed using VTK [51] and Qt [52] libraries, used to display the acquired triangulated mesh, to select on a sort of electronic record measurements names, placing on the mesh the required markers for each measurement.

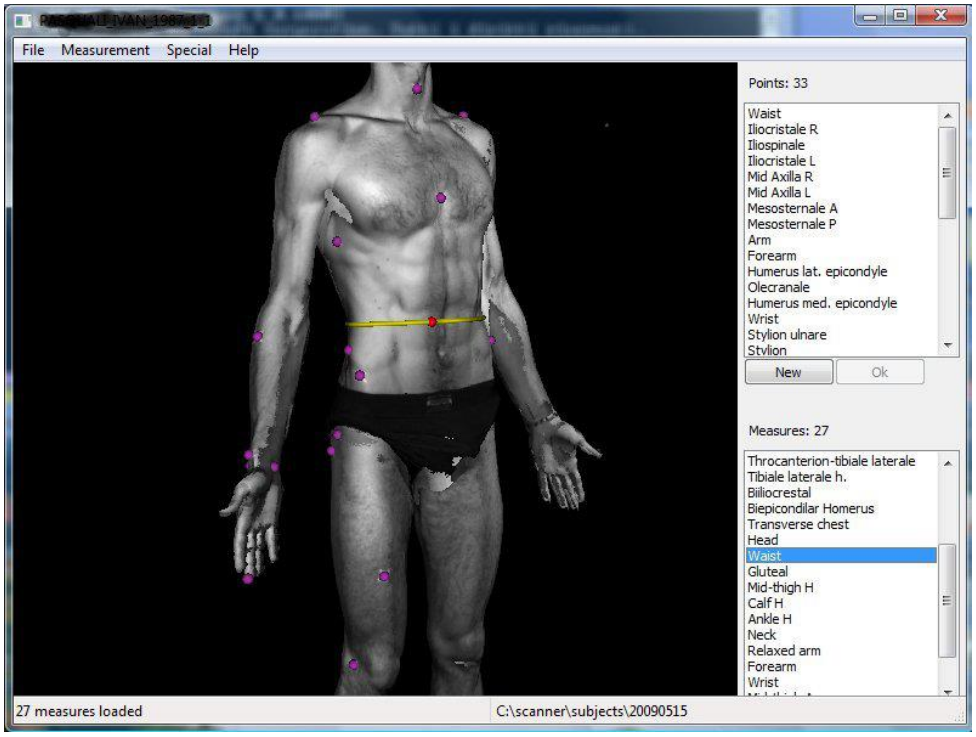

Figure 5: User interface of the computer assisted measurement system.

The fit of the stick figure over the curve skeleton obtain head, trunk and limbs size and orientation reducing possible errors in the skeletal feature location. In order to perform all the standard measurements required the user has the possibility of selecting one or more points on the surface and estimate from them different kind of meaures:

- Height (distance from floor)
- Distances between selected points
- Girths passing through a point, parallel to floor or perpendicular to a skeletal line
- Geodesic paths joining two or more points

Figure 6 shows examples of measurements performed on the user interface.

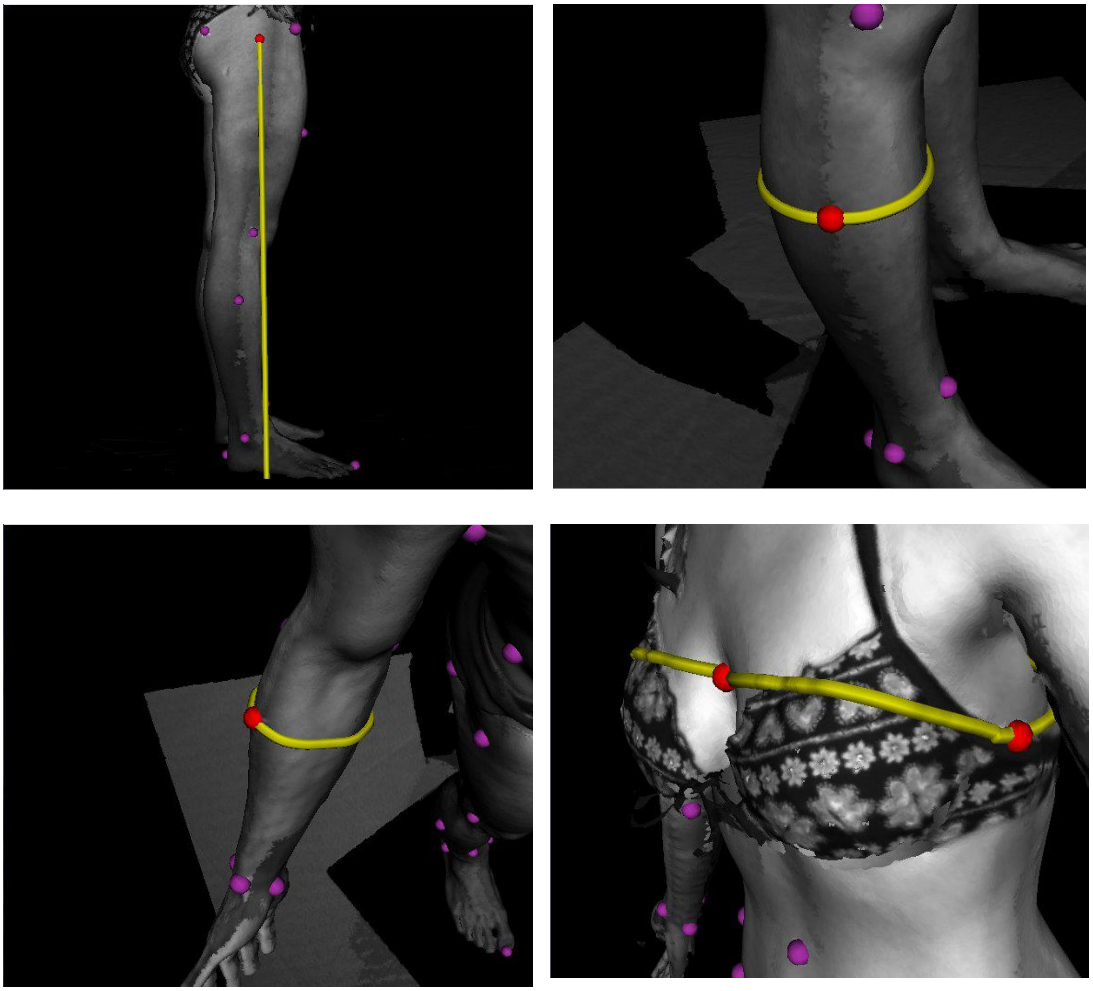

Figure 6: Examples of measurements performed interactively with the user interface. Landmarks positioning or section plane angles can be interactively modified.

Examples of length/distances (which calculation from terminal points coordinates is straightforward) are: Radiale-stylion,Midstylion-dactylion,Iliospinale h., Trochanterion h., Throcanterion-tibiale lat., Tibiale lat. h., Foot length, Biacromial, Biiliocrestal, Transverse chest, A-P chest depth, Biepicondilar humerus, Wrist breadth, Bimalleolar breadth. Examples of girths are: Head, Neck, Arm, Forearm, Wrist, Chest, Waist, Gluteal, Mid-thigh, Calf and Ankle.

The evaluation of girths requires often the extraction of section planes perpendicular to the limbs (or neck or trunk) direction. Although most of the girths are parallel to pavement, in order to be more accurate we use, for some of the measurement, the information extracted

with the skeleton/stick figure. This make the system more robust against changes in the standard pose of the subject with respect to other methods.

For the simulation of tape measures that cannot be assumed as “planar”, as in the chest girth, we used a different girth computation approach, i.e. through the geodesic path. The computation of geodesic paths joining a set of landmarks on the original mesh can create some problems due to the fact that the meshes obtained from the bodyScan are not clean and watertight. In order to obtain accurate measurements we therefore developed an algorithm to approximate geodesic distances on the mesh that can handle holes and discontinuities in the body surface. It is based on the computation of distance maps computed on the surface: when the mesh presents borders, the map at each border point is updated as the minimum between the current value due to the node propagation, and the sum of values at other points of the same contour border and the Euclidean distance between points.

With the user interface developed it is easy to simulate interactively the measurement procedures usually performed manually on the subjects. It is sufficient to select the name of the standard value on an electronic record, select the landmarks related with that measurement clicking on the model surface on the interface, check the measurement path drawn in the scene and saving the value if everything is correct.

The landmarks used for the anthropometric measurements are marked on the skin of the subject drawing a with a dermographic pen before the acquisition. The placement of such landmarks is useful for several reasons:

- it allows the offine measurement on the mesh of values landmarks that cannot be located using image based or geometrical features. Relevant measurements, in fact, are based on landmarks placed by physically touching the subject.
- it allows an easier semi-automatic placement of the points during the computer based measurements.
- reference points can be used to validate automatically the landmark detection algorithms based on surface features.

During the measurement process, the user should click on the mesh in concomitance of the visible cross and label the traced point.

For each simulated measurement, the interface shows the selected points on the skin, and all the lines, geodesic paths and sections used for the value estimation. During the process, users can always change landmark positions, and, if the measures depend also on the automatically extracted section planes, it is possible to correct manually the plane orientation.

Obtained measures can finally be exported on a spreadsheet for further analysis.

Manual anthropometry

A set of 28 anthropometric parameters was chosen to include most of the current circumferences, lengths, and widths taken in anthropometric surveys (Table 1). Measurements were performed on two different occasions by one experienced anthropometrist (CM) according to standard procedures [53].

The body sites were marked prior to measurement using a dermographic pen; such landmarks were found to be easily visible in 3D scanning images in preliminary experiments.

Table 1. The set of anthropometric parameters measured in this study.

Type of measurement	Body Site/measure
Circumferences	Head Neck Arm (relaxed) Forearm Wrist Chest Waist Gluteal (hip) Mid-thigh Calf Ankle
Lengths/heights	Shoulder-Elbow Radiale-stylion Midstylion-dactylion Iliospinale to floor Trochanterion Trochanterion-tibiale laterale Tibiale laterale Tibiale-sfirion tibiale Foot
Widths	Bi-acromial Bi-iliocrestal Chest (transverse) Chest (A-P) Bi-epicondilar (humerus) Wrist Knee Bi-malleolar

Digital anthropometry

The experienced anthropometrist was instructed to perform digital anthropometry on 3D images of the twelve subjects using the same landmarks as for manual anthropometry. Manual measurement procedures have been simulated through the development of a user friendly measurement interface that enables the operator to easily place landmarks on the virtual body surface and automatically obtain the related set of measurements. Our dedicated software tool is based on the the VTK library[51] and exploits for the measurement procedures an

automatic mesh processing that pre-computes body posture and limb directions and recognize the main body parts [54].

All measurements were obtained in duplicate. Two naïve anthropometrists carried out the same procedure independently from each other.

Statistical analysis

Descriptive statistics were calculated for all variables (measurements) by each method (manual/digital). Normality of data was assessed with the Kolmogorov-Smirnov test. Reliability of measurement was assessed by calculating the product-moment Pearson's correlation coefficient, the Student's t test (two-tailed), and the intraclass correlation coefficient (ICC; Crombach's alpha using a mixed model [type: consistency]). All statistical analyses were performed with the SPSS package (v. 15). The level of significance for all statistical tests was set at P=0.05.

Experiment 2

Health-related shape analysis

We analyzed data from 25 obese otherwise healthy female subjects, aged 20-60 years and BMI 30-40 kg/m². The subjects underwent DXA scanning, optical 3D scanning and standard anthropometric procedures [1]. During scanning and anthropometry, subjects wore close-fitting underwear. During DXA examination subjects wore light garment, transparent to X-rays.

For every single subject, 3D scanning, DXA and manual anthropometry were performed sequentially in one session.

DXA scanner

Dual-Energy X-rays absorptiometry represents the de-facto standard measuring tool for body composition analysis. It allows to assess body composition in terms of fat, lean and mineral mass at the total body as well as regional level [55]. The DXA device used in this experiment is the DXA QDR Explorer W (Hologic, MA, USA) of the faculty of Motor Sciences of Verona University. The body composition assessment consists of an acquisition step and a subsequent definition of body regions on the 2D acquisition performed by an operator (Figure 7).

Main results of DXA analysis consists in whole-body composition parameters and regional composition data. For our experiments we chose three parameters:

1. Trunk Fat

2. Subtotal Fat

3. Subtotal Fat Percentage

Trunk Fat is the total fat detected in the trunk region (as defined by the operator according to stringent anatomical landmarks on the 2D acquisition); Subtotal Fat and Subtotal Fat Percentage refer to the fat of the whole body without the head; the reason for that is large amount of mineralized tissue in the skull, preventing reliable evaluation of the head fat component. Those last two parameters are well-known risk factors for metabolic alterations and disease.

Figure 7. Whole body composition (BC) images output of a DXA exam. On the left: BC in false colors. On the right: regions setting by means of template defined by colored lines (source: Hologic)

Human Analyzer Tool

Automatic computation of geometrical parameters from generic body scanner data was performed with a specifically designed software tool, able to load 3D meshes and provide directly geometrical parameters without the necessity of user intervention.

It performs a preprocessing step able to remove spurious parts of the model and creating a new watertight mesh with the Poisson algorithm. This procedure is based on VCG/Meshlab scripts [56], integrated in the software package, implemented for the other parts with custom C++ code.

The subsequent segmentation procedure has been derived from the method described in [57], that is based on a curve skeleton extraction and its partitioning based on the extraction of features on the major skeletal leaves. In this way it is possible to detect and recognize points where head and limbs join the body trunk. This procedure is however not precise when the captured shape is not optimal, e.g. arms are partially attached to the trunk or legs are in contact under the crotch; these problems are often encountered when dealing with obese subjects.

For this reason we modified it by using special heuristics to refine the position of the feature points used to define the body segmentation, e.g. attachments of limbs to the trunk.

First of all, we observed that, where legs and arms are attached to the trunk, their direction should be approximately parallel to the trunk axis. This means that we can use the detected endpoints of the limbs to define a plane approximately including the trunk axis, so we can define an approximate trunk axis, and approximate transverse and antero-posterior directions.

We then move the detected leg centerline endpoints toward the trunk until the antero-posterior distance along the line joining the leg centerline endpoints is not lower than at its extrema.

We adjust then the crotch position and the trunk axis direction analyzing the trunk sections perpendicular to the previously detected axis near detected endpoints.

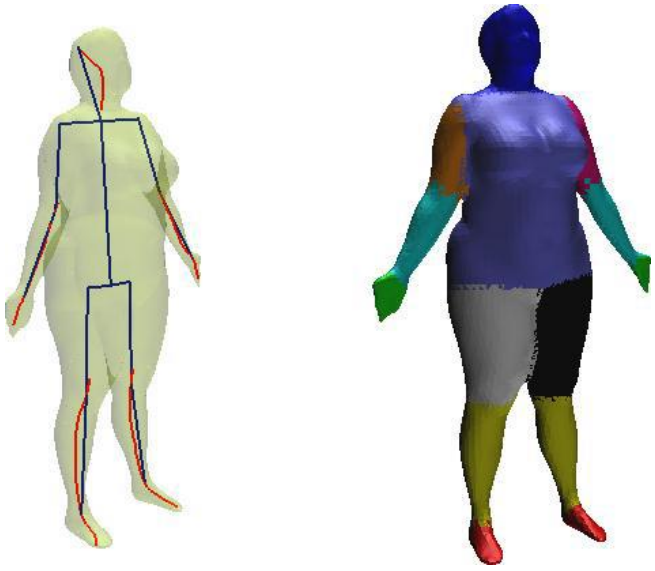

Figure 8. Left: segmentation based simply in the extrema of tubular parts (defined by red centerline paths) fails in capturing the real position of limb endpoints due to the attachments of limb to the trunk. With the simple heuristics describe in the text our software can locate the correct position and obtain a reasonable stick figure (blue), body part segmentation (right) and the estimate of the axial, antero-posterior and transverse directions useful to evaluate the parameters considered in our study.

Lateral trunk limits (transverse distance from the axis) are obtained detecting the lower part of the arms branching and symmetrizing the result, finally the shoulder position is searched as the upper points of the intersection of the planes defining these limits with the trunk geometry.

Figure 8 shows an example of automatic body segmentation result with the curve skeleton, its initial partitioning, the refined limb extrema defining a reasonable stick figure even for overweight subjects.

Known the body segmentation, the trunk centerline, transverse and antero-posterior directions, we can compute a number of parameters (lengths, girths, volumes, etc.), with accuracy that is obviously depending on acquisition protocols, body position, etc. In this work we selected a few parameters that we assumed could be reasonably accurate correlated with the body fat.

The software tool performs the automatic evaluation of the parameters (saved as a text file) as well as a segmented 3D surface, the computed curve skeleton and stick figure.

Most trunk measurements are made by means of analysis of profiles curves along trunk centerline, so that every profile point characterizes a trunk slice.

Typical profiles measures are antero-posterior diameter, latero-lateral diameter, mean diameter, eccentricity and curve length (the equivalent of “Circumference” in anthropometry) of the slice (Figure 9).

In this way is simple to derive meaningful geometrical measures, like maximum antero-posterior diameter or maximum curve length.

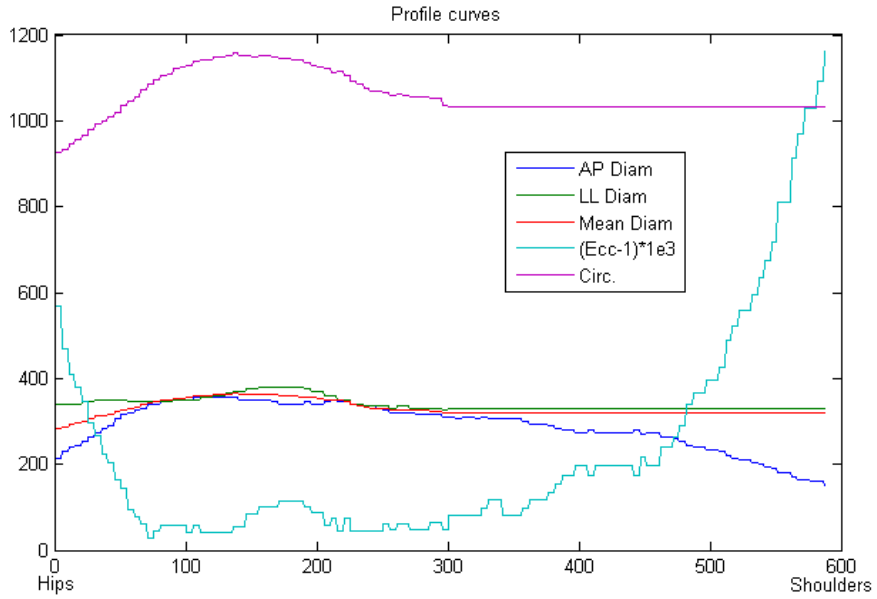

Figure 9. Example of computed profile curves on the trunk. The curves represent antero-posterior, latero-lateral and mean diameters, eccentricity and slice circumference Eccentricity (maximum and minimum diameters ratio) profile has been rescaled for clarity.

Data comparison

We performed the comparison analysis of DXA data with automatic and manual measurements using Pearson's linear correlation coefficient.

Chosen DXA measurements were trunk fat, subtotal body fat and percentage of the former over subtotal body mass. Body composition parameters have been correlated with some standard anthropometric indexes and circumferences. Standard indices are usually employed to evaluate the health status of individuals. Some of them, like BMI and body mass are known to be correlated with fat parameters, because fat mass directly influence them.

We compared then the same DXA parameters with the digital measurements performed on 3D mesh summarized in Table 1.

Table 1. Description of performed automatic digital measurements

Name	Description
AP max	Maximum anteror-posterior diameter
MD max	Maximum mean diameter
Area max	Maximum of slice area
Height/MD ratio	Ratio between the height of the trunk (hips-shoulders height) and the maximum mean diameter. This measurement gives a gross shape description of the trunk proportions
Trunk vol.	Volume of the whole trunk, computed as sum of the slice areas
Abdomen subvol.	Volume of the lower part of the abdomen, from hips to height of max AP
Min/max circ ratio	Ratio between minimum and maximum curve lengths
Min/max area ratio	Ratio between minimum and maximum slice areas
AP curv.	Curvature of the AP curve in the neighborhood the maximum value
MD curv.	Curvature of the MD curve in the neighborhood the maximum value
Circ. curv.	Curvature of the Circumference curve in the neighborhood the maximum

We conceived the set of measurements to capture in various ways the trunk geometry. Some of them are similar to the standard anthropometric ones; some others are instead almost impractical with standard anthropometry.

We also focused on measurements that are reasonably not affected by inaccuracies in mesh acquisition and processing, as it would happen if they are performed in regions where the original mesh presents holes.

Experiment 3

Multiscale Area Projection Transform

Most biological objects presents parts that grossly presents radial symmetry (e.g. spheres, cylinders). The detection and description of this kind of shape could be therefore useful for a variety of shape analysis tasks applied to the 3D description of biological objects.

We present a new spatial transform called multiscale area projection transform (MAPT) measuring the local likelihood of points in 3D space to be centers of radial symmetry at selected scales. The transform can be easily estimated on triangulated meshes and can be used not only to detect salient points and to reconstruct centerlines of tubular shape parts, but also to characterize globally the shape: its histograms are able to capture invariant features of rigid and articulated bodies and can be used for shape retrieval, comparing very well with state of the art techniques. Moreover, joining the detected salient points through paths that follows maximal values of MAPT allows to build graphs that can be used to extract relevant shape properties of complex articulated models.

Area Projection Transform

Our basic idea is to compute from input surfaces a spatial function that is maximal near centers of approximately spherical surfaces with a selected radius R and along centerlines of tubular structures with approximately circular section of radius R, so that it can be used to locate salient points and regions characterized by radial symmetry. This result can be obtained by projecting surface points along the local normal vector $\vec{n}$ at distance *R*. The likelihood of a point $\vec{x}$ to be center of a radial symmetry can then be assumed to be proportional to the number of points of the original surface S that are projected in a neighborhood of $\vec{x}$ or, in other words, to the area of the original surface projected in that neighborhood. To compute this point density for a generic surface S in the 3D space, we consider the transform $T_R(S,\vec{n})$, creating a correspondence between S and its "parallel surface" [58] at the distance R on a selected side (moving each point of S along the normal direction $\vec{n}$, see Figure 10). For each point $\vec{x}$ in $\mathbb{R}^3$, a sphere with radius σ centered in $\vec{x}$ includes a subset of the surface $T_R(S,\vec{n})$, that is ks(~x) $k_\sigma(\vec{x}) \subset T_R(S,\vec{n})$; we define "area projection transform" APT(~x,S,R,s) the area of the subset of S having its parallel surface inside the sphere:

$$APT(\vec{x},S,R,\sigma) = Area\left(T_R^{-1}\left(k_\sigma(\vec{x}) \subset T_R(S,\vec{n})\right)\right) \quad (1)$$

If we want to characterize both the sides of the surface we can compute also the contribution of the other parallel surface at distance R. i.e. $T_{-R}(S,\vec{n})$, possibly with opposite sign to separate the different kinds of features. T_R is well defined for continuous surfaces (properties of parallel surfaces can be found in [58]), and this is not always the case of data captured by scanners or reconstructed from volumetric grids. However we can easily compute the APT as the sum of the contributions of all the continuous patches acquired. If we can assign a common orientation to the patches we can compute the transform only for a selected

orientation (e.g. inside the object), otherwise we can compute the APT as a sum of the contributions of the two sides.

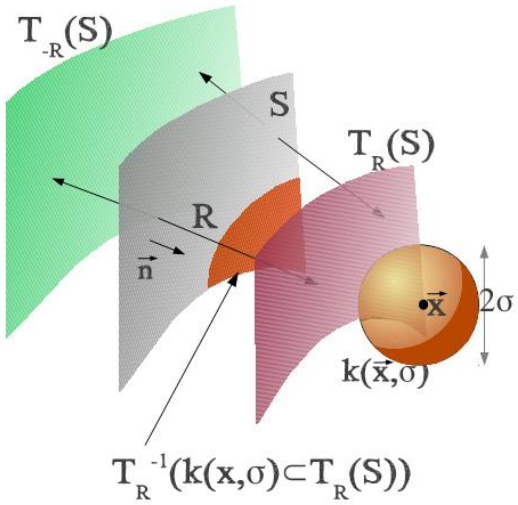

Figure 10: Basic idea of the area projection transform: we compute the parallel surface at distance R (only in a selected direction or both directions) and we compute the transform in a point $\vec{x}$ as the area of the original surface generating the part of the parallel one falling inside a sphere of radius s centered in $\vec{x}$.

It is easy to understand why this transform captures radial symmetry: a spherical surface with radius R projects all its surface on a single point and the APT is non-negligible only within a distance s from this point (see Figure 11). A similar reasoning can be done for cylindrical surfaces. Radial symmetries will determine maximal regions for the APT and the value of σ determines the deviation from a perfect symmetry we want to tolerate when detecting it. Furthermore, exact values of the expected maxima of the APT in the case of spheres or cylinders can be computed: if the surface S is a sphere with radius R and we compute the APT with the same R, the expected value near the center is the area of the spherical surface $4\pi R^2$, independently on the choice of σ (Figure 11).

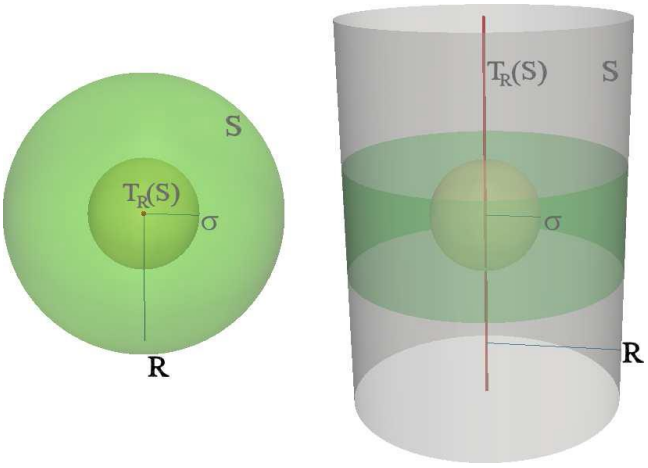

Figure 11: Left, the internal parallel surface at distance R of a sphere S with radius R collapses in the central point. The maximal value of the APT computed exactly at scale R is the area of the entire spherical surface, i.e. $4\pi R^2$. Right: for a cylindrical surface of radius R the internal parallel surface at distance R collapses into a line. The APT computed at scale R has a maximal value along that line equal to the area of the green part of the cylinder, $4\pi R\sigma$.

If we make the value of s tend to zero, we can consider

$$\rho_{AP}(\vec{x}, S, R) = \lim_{\sigma \to 0} \frac{APT(\vec{x}, S, R, \sigma)}{{}^{4}/_{3}\ \pi\ \sigma^3} \tag{2}$$

a density function in R3 measuring the amount of points of the original surface mapped in each infinitesimal region of the parallel surface. We can, in this way, reinterpret the APT as a kernel density estimate of ρ_{AP} with a unitary spherical kernel of size σ that could, in principle replaced by an arbitrary kernel in a generalized APT definition.

Handling multiple scales

When we search for radial symmetry we do not usually want to do it for a fixed R, but we want to find features at different scales. If we consider the radius R as a fourth variable in previous definitions, we obtain immediately multiscale versions of APT and ρ_{AP}. However, in order to compare the values at different radii and correctly characterize the scale of the dominating symmetries, a good idea is to define a multiscale area projection transform (MAPT) with the following two properties:

i) a perfect sphere creates a signal with values in its center independent on its radius;

ii) two surfaces differing for a scaling transform have the same maximum.

These properties are obtained with the following definition:

$$MAPT(x, y, z, R, S) = \alpha(R) APT\big(x, y, z, S, R, \sigma(R)\big) \tag{3}$$

where $\alpha(\mathrm{R}) = 1/4\pi\mathrm{R}^2$ and $\sigma(\mathrm{R}) = \mathrm{c} \cdot \mathrm{R}\ (0 < \mathrm{c} < 1)$.

The coefficient a makes, in fact, a perfect sphere create a central value equal to 1 independently on the radius. The choice for σ makes a shape scaled by a factor k produce a MAPT maximum at scale kR equal to the maximum of the original one at scale R. The resulting MAPT characterizes therefore the shape with values depending on the degree of radial symmetry independently on the scale. We know also that maximal value in center of perfect spheres should be equal to 1, while cylindrical shapes, following the reasoning of Figure 11, should be characterized by maxima equal to $2\pi\mathrm{R} \cdot 2\mathrm{cR}/4\pi\mathrm{R}^2 = \mathrm{c}$, still scale independent, but depending on the kernel size. A search for similar salient symmetric locations on input surfaces can be then performed on the 4-dimensional MAPT estimated for a reasonable range of radii, and can be also performed with a joint multiscale approach, combining the maps computed at different scales in an unique saliency function (joint multiscale APT). This map can be defined as:

$$\mathrm{JMAPT}(\mathrm{x}, \mathrm{y}, \mathrm{z}) = \max_R(\mathrm{MAPT}(\mathrm{R})) \tag{4}$$

and should still encode the main features related to the shape symmetry, even if it is clearly less informative than the 4D function. However, its use reduces the amount of memory required, that can be huge if the discretization is fine. Note that if we search for symmetric points on the JMAPT, in order to be able to recover their scale, it is useful to create an

additional matrix SMAPT(x, y, z) storing the related scale information, e.g. the radius corresponding to the maximum of MAPT(x, y, z,R) at each spatial location.

MAPT and the medial axis transform

Our transform is also related to the medial axis of a surface [36], e.g. the locus of centers of spheres tangent to it in at least two distinct points, widely applied in geometrical processing. Actually the joint multiscale APT, defined in Sec.4, when the kernel radius tends to zero, vanishes with the exception of the points where there is an exact spherical symmetry of a surface part. These points are clearly a subset of the medial axis (centers of spheres tangent to the surface in an infinity of points), where the limit values of the function give further information related to the spherical parts area values. If we count the area elements projected into the kernel volume and consider the set of points where in the limit s!0 the number is greater than 1, we can obtain the rest of the medial axis as a limit case from the JMAPT. Being possible to enrich the JMAPT with the associated scale, we can actually obtain the complete MAT from it.

In some sense we can consider the JMAPT an approximated and volumetric version of the medial axis transform. It is also a robust representation being not much changed by small perturbations of the surface (while the medial axis is completely changed by small bumps even far from them).

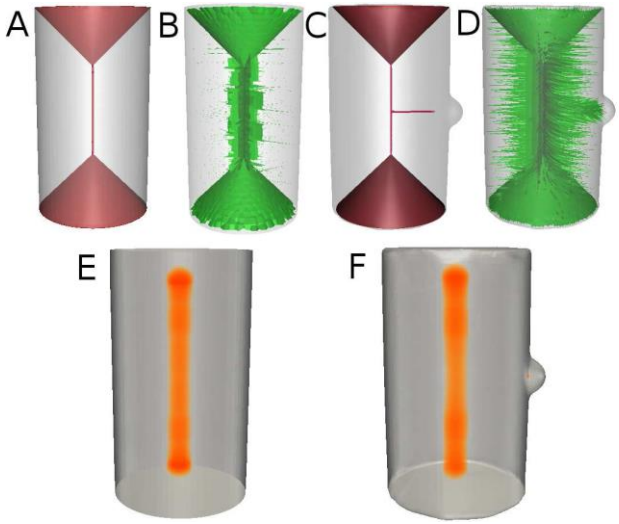

Figure 12: The medial axis of a cylinder includes also cones at the extrema (A) and when a small spherical perturbation is produced on it a complete line appears (C). This makes its computation on discretized surfaces not stable (B,D, computed with public code from [44]) The Joint MAPT is related to the medial axis (see text), but, weighting the area approximately tangent to spheres, it is not high in non-symmetrical regions near the bases of the cylinder (E) and, adding the small spherical perturbation, only the center of the sphere presents relevant values in addition to the axis.

This fact can be understood looking at Figure 12: the ideal medial axis estimated on a cylinder is a segment only far from the bases, where it is transformed in two conic surfaces (A). If a small perturbation is added, a new complete branch appears even if no tubular parts are present (C). Due to this low stability, algorithms for its numerical estimation on meshes provide noisy results (B,D). The ideal JMAPT for a cylinder should be maximal on the axis and decreasing around it with a behavior depending on the selected parameters.

The JMAPT computed with our code on an approximately cylindrical mesh has the expected appearance (E). After the "spherical" perturbation, the JMAPT is relevant still on the axis in the center of the spherical bump, but is low elsewhere due to the negligible projected surface (F). The robustness provided by the local weighting of the symmetric surfaces is different from that provided by robust variants of the medial axis. For example the l-medial axis [59] is obtained removing centers of spheres with radius lower than a threshold and the scale axis transform [60] creates medial surfaces at different scales by extracting medial axes on shapes

simplified by "multiplicative scaling" where radii of medial balls are changed. Using the APT maps we can as well select "medial representations" at different scales, but we have also the relevance given by the projecting surface area. Our volumetric density cannot replace medial surface representations having different nature and applications. However, the use of the MAPT as importance and scale-selective weight for medial axis branches could be investigated.

Centers of Approximate Spherical Symmetry

Give the MAPT or the JMAPT of a shape, it is possible to extract its salient points, e.g. maxima of the 4D or 3D map. The procedure is rather simple. After a non-maxima suppression is performed, local maxima are sorted, and those lower than a threshold and those closer to another maximum with higher value and of similar scale more than the corresponding radius are removed from the list. The extracted points represent loci of maximal "approximated" spherical symmetry where the parameter σ(R) used in the Area Projection Transform defines the amount of deviation from the perfect sphericity that is tolerated.

A good property of these points is that they are approximately pose independent for articulated shapes and roughly corresponding in similar bodies. We can easily associate a descriptor to these points computing five local features. The first two are the local intensity of the map and the related scale. The other three are related to the local orientation of the projecting surfaces in the neighborhood of the point, e.g. the sphericity, elongation and flatness of the map in a neighborhood proportional to the local scale, evaluated from the inertia matrix of the MAPT. Another way to estimate local orientation is to collect not only intensity projected by sampled points on the surface when building the MAPT on a discretized grid, but also direction, at the cost of a huge memory overhead (a tensor for each location and each scale must be stored). This description can be sufficient to recognize specific points of a shape (e.g. head or trunk of a human body that have unique scale or peculiar sphericity), but is

clearly not sufficient to allow a reliable point matching between two corresponding shapes. To create a good characterization of points and a global model description we can, however, join the points, buinding a graph representation. Our idea is to join the salient points following maximal symmetry path, in this way following centers of approximately cylindrical parts independently on the quality and on the topology of the shape borders.

Radial Symmetry Graphs

We therefore create our "Radial Symmetry Graph" from the CASS points with the following procedure:

- Join each point of the list with all the others by performing fast marching from the points with speed proportional to the squared symmetry scaled value mapped in the range 0.001 − 1 and extracting minimal paths [61]. This results in lines that tends to follow cylindrical part axes when available otherwise follow minimal euclidean paths.
- (optional) Clean the graph by removing all the paths that are close to another CASS point different from its extrema. The structure obtained has some interesting properies:
- It follows tubular parts of the shape: as shown in [62] the JMAPT is maximal along cylindrical paths, also robustly against noise and holes.
- It tends to connect these cylindrical centerlines to centers of spherical structure or to corners (creating an approximate spherical symmetry as shown in [62])
- relevant information is encoded in paths. We can use, to match points or entire graphs, not only the information related to node features or to connectivity, but also path similarity, as, for example, done in [63].

An example of a shape with its generated radial symmetry graph is showed in Figure 13

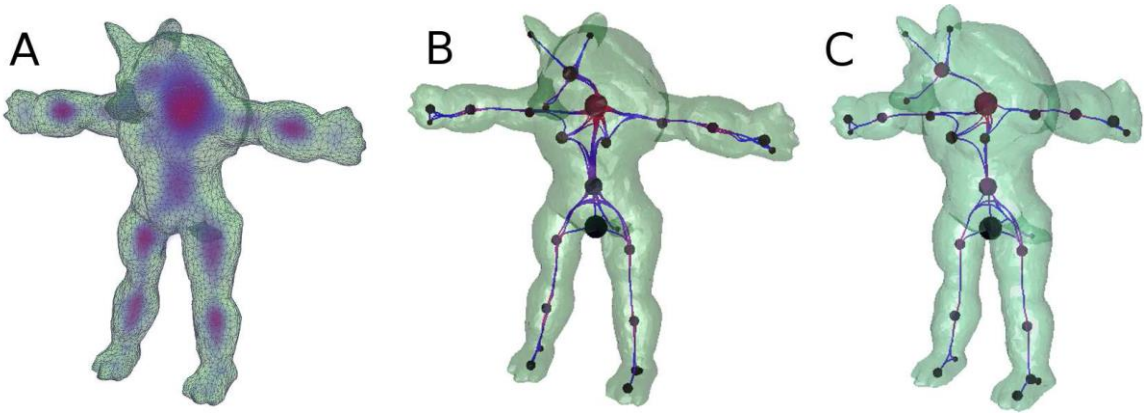

Figure 13: A: Volume rendering of the JMAPT computed on an armadillo mesh. B: CASS points extracted from the map represented as spheres of 1/4 of the corresponding scale, rendered with color coded sphericity and Radial Symmetry Graph joining all the points. C: Same radial symmetry graphs simplified by removing paths too close to salient points different from their extrema.

Note that the complete graph characterize points (and can be used also to characterize entire shapes) only through the path behavior. The cleaned graph can describe the global object properties also through its connectivity.

Comparing paths connecting CASS points we have a powerful way to characterize locally and match salient points and to match complete graphs. Following the approach of [63] we can, in fact compute path dissimilarity by summing two contributions. The first depends on symmetry scale difference in N evenly spaced points along the paths ($\overrightarrow{p_1}(i)$ for the first path and $\overrightarrow{p_2}(i)$ for the other one). The second depends

on the difference of the paths lengths l1, l2:

$$d(p1,p2) = \sum_{i=1}^{N} \frac{(S_{MAPT}(\overrightarrow{p_1}(i)) - S_{MAPT}(\overrightarrow{p_2}(i)))^2}{S_{MAPT}(\overrightarrow{p_1}(i)) + S_{MAPT}(\overrightarrow{p_2}(i))} + \alpha \frac{(l_1 - l_2)^2}{l_1 + l_2} \quad (4)$$

Actually to compare our paths we could add also also a JMAPT intensity based dissimilarity component:

$$d'(p1,p2) = \sum_{i=1}^{N} \frac{(JMAPT(\overrightarrow{p_1}(i)) - JMAPT(\overrightarrow{p_2}(i)))^2}{JMAPT(\overrightarrow{p_1}(i)) + JMAPT(\overrightarrow{p_2}(i))} \quad (5)$$

Scale information, however, should be more robust against holes with respect to signal intensity so it is reasonable to omit the intensity component directly depending on the amount of surface projected in the point. Lengths and scales should be approximately pose independent and characterize well the shape.

Once salient points, graphs, paths and path comparison metrics are available, we can use them for at least three practical applications, that give the basis for automatic shape analysis: point matching, semantic labelling of point, graph matching and intrinsic symmetry detection. The approaches we are trying to follow for these tasks will be shown in the results.

3. Results

Here are reported the main results of our research. Firstly we validated the anthropometry procedures performed through Breuckmann BodySCAN. The second result consists in the comparison of newly-obtained semi-automatic measurements method with other health related physiological parameters, i.e. total and regional body fat. Finally, we present some experiments of mesh analysis performed for test of Area Projection Transform. We applied to research on this method in order to overcome the problem of "hole sensitivity" presented by most of the conventional tested methods. Nevertheless there aren't yet direct applications of anthropometry, it offers good perspectives for the development of robust algorithms for mesh analysis which could lead to new robust procedures of tridimensional morphometry.

Experiment 1

Validation of the Breuckmann BodySCAN

Manual Anthropometry

Manual anthropometry showed intraobserver correlation coefficients r for duplicate measurements in the range 0.975-0.999 ($P<0.0001$ for all) but for mydstilion-dactylion ($r=0.781$, $P=0.003$); the Student's t test (two-tailed) showed that mean values of duplicate measurements for individual anthropometric variables were not significantly different by two-tailed t test with the exception of mydstilion-dactylion (188.08± vs. 186.17± mm; $t=8.815$, $P<0.001$) and tibiale laterale to floor (453.17± vs. 451.83± ; $t=2.402$, $P=0.035$) as well as, at the

limit of significance, bi-iliocrestal (284.58± vs. 283.25± ; t=2.111, P=0.058); and wrist width (54.50± vs. 55.17± ; t=2.152 P=0.054). The ICC was in the range 0.955-0.998 (P<0.0001) with Cronbach's alpha ranging 0.977-0.999.

Digital anthropometry

Duplicate measurements taken digitally by one experienced anthropometrist and two naïve anthropometrists showed intraobserver correlation coefficients r in the range 0.975-0.999 (P<0.0001 for all). Mean values of duplicate measurements for individual anthropometric variables were generally not significantly different intraobserver by two-tailed t test. The ICC was in the range 0.759-0.999 (P<0.001-P<0.0001) with Cronbach's alpha ranging 0.863-0.999. Most measures taken by the experienced anthropometrist in the manual and digital mode showed ICC ranging 0.855-0.995 (Krombach's alpha 0.959-0.999), p<0.0001 for all; lower, albeit significant, ICC values were found for head circumference (0.446; alpha 0.763 P<0.001), wrist circumference and breadth (0.678 and 0.654, respectively), bi-epicondilar humerus (0.695; alpha 0.901).

Experiment 2

Health-related shape analysis

We used our custom software tool to extract the measurements listed in Table 1 on the digital models captured by the 3D scanner. Computation time is less than on minute per model on a Dell XPS17 laptop with an Intel Core I7 Q740 CPU and 8Gbyte of RAM, running Ubuntu Linux.

The resulting measurement reports were then imported in Matlab, together with DXA data and manual anthropometry measurements in order to perform statistical analysis.

In Table 2 Pearson's Correlation coefficients between three DXA body composition parameters and the anthropometric (standard and digital) measurements are shown.

Table 2. Correlationm matrix of anthropometric measurements and DXA trunk fat, subtotal body fat, and % subtotal body fat

DXA Parameter / Anthropo-metric Item	Trunk Fat	Subtotal Fat	% Subtotal Fat
BMI	0.8379	0.8466	0.4698
Weight	0.8314	0.8693	0.3542
Hips C.	0.7757	0.8970	0.6188
Waist C.	0.7573	0.4793	-0.0208
W/H ratio	0.1587	-0.2259	-0.5192
AP max	0.9128	0.7616	0.3877
MD max	0.9316	0.8894	0.5224
Area max	0.9367	0.8794	0.4838
Height/MD ratio	0.5995	0.6235	0.5326
Trunk vol *	0.6196	0.2025	0.0495
Abdomen subvol	0.0863	0.3813	0.4183
Min/max circ ratio	0.3221	-0.0272	-0.1023
Min/max area ratio	-0.2865	-0.0325	0.0813
AP curv.	-0.3148	-0.3559	-0.3165
MD curv *	-0.3611	-0.0840	0.0704
Circ. curv *	-0.3110	-0.1948	0.0451

* Some outliers removed (see text)

In three cases we took out from statistics one or two outliers (one from Trunk vol. and two from the curvatures). The table is subdivided in three groups of rows. In the first group, correlations with standard anthropometric measures are shown. The second group presents digital measurements that are strongly correlated with DXA measured fat. The third group shows digital measurements that are poorly or not correlated with DXA data.

In figures 14 and 15 the scatter plots for the firs and the second groups of measurements are shown.

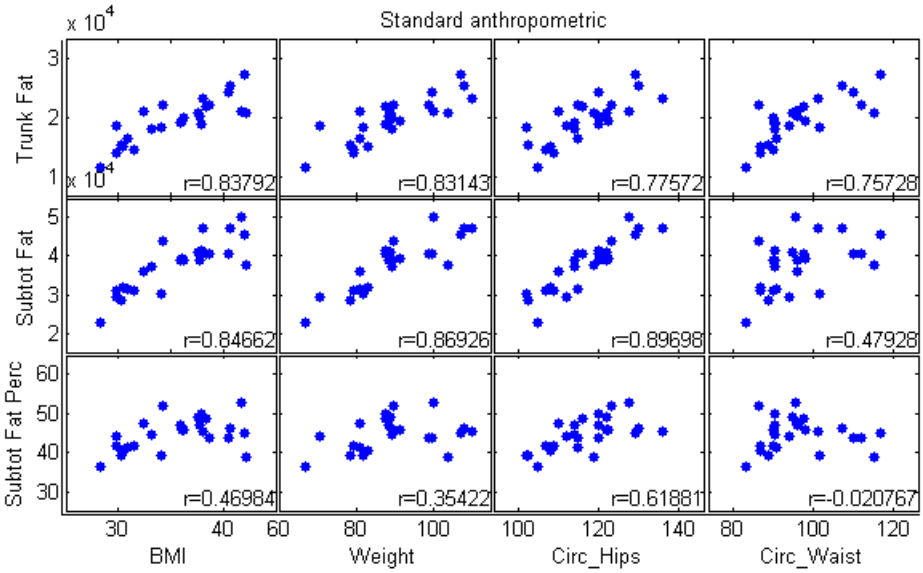

Figure 14. Scatter plots of standard anthropometric measurements vs. DXA measurements. Pearson's Correlation Coefficients are indicated

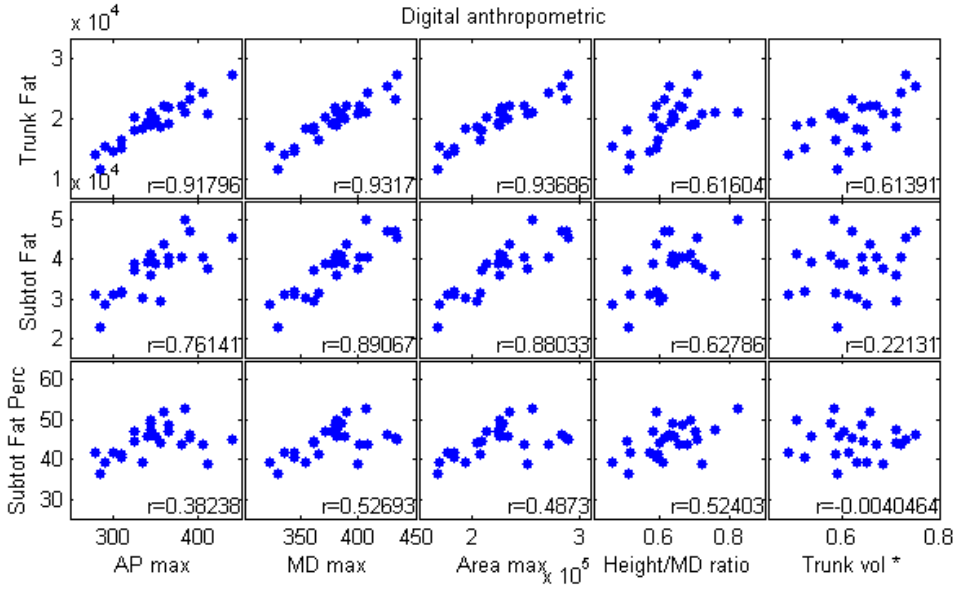

Figure15. Scatter plots of selected digital measurements provided by the Human Analyzer software vs. DXA measurements. Pearson's Correlation Coefficients are indicated

Looking at results of standard measurements, we can see that BMI and body weight are well correlated with trunk and subtotal fat, as expected. Also hip circumference presents a high correlation index with subtotal fat.

As to digital measurements, there is a very high correlation (>0.9) of AP max, MD max and Area max with Trunk Fat, while the correlation with Subtotal Fat is high, but not as high as with Trunk Fat. Height/MD ratio and Trunk Vol correlate less ($r \simeq 0.6$) with fat measurements.

As to the Subtotal Fat Percentage, correlations with evaluated standard and digital measurements are almost weak. Best found correlated measurements are $r \simeq 0.6$ with Hips Circ. and $r \simeq 0.5$ with MD max, Area max and Height/MD ratio.

Experiment 3

Area projection transform : applications and experiments

Here we give some examples to show their practical useful applications of the APT algorithm presented in chapter 1, showing some of its properties and its proficiency performing some mesh analysis tasks. We will not show the application only to human-shaped meshes, but to standard meshes got from open bases of shapes which contains meshes which specific properties (e.g the armadillo in different poses). In figures 16 and 17 the values of APT for different shapes and radiuses are shown.

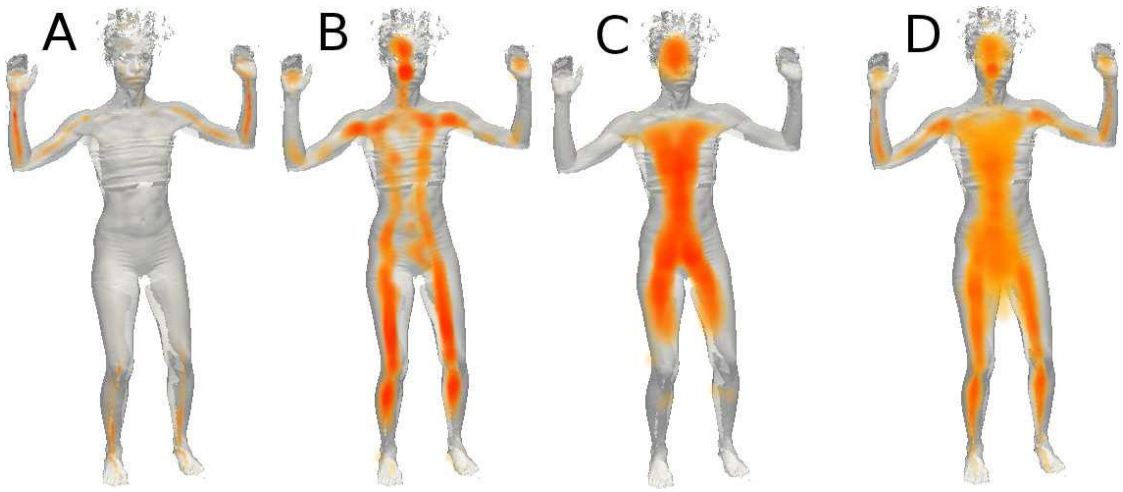

Figure 16: The ability of MAPT to enhance centers of radially symmetrical parts is evident also in the case of noisy captured meshes with large holes, as in the case of this whole body human scan. Volume rendering of APT at three different scales (A,B,C) and of JMAPT (D) are shown.

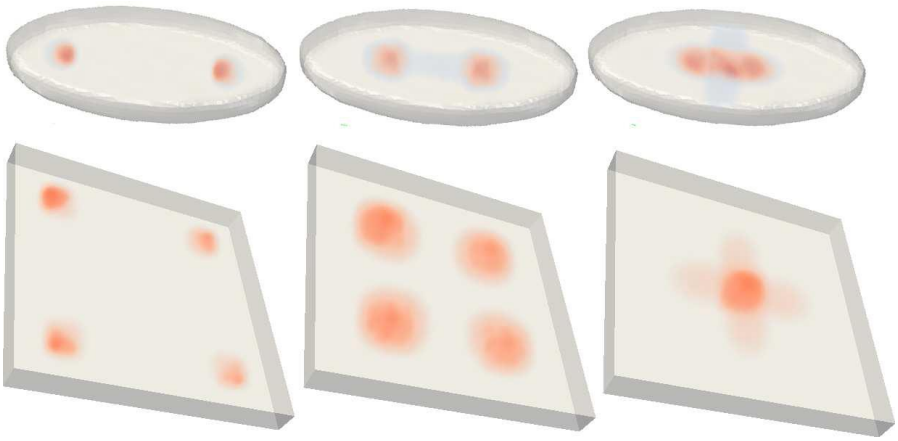

Figure 17: APT at different scales creates peculiar structures also on flat and non-spherical or tubular objects.

Salient points detection and characterization

Salient points related to high radial symmetry can be extracted as local maxima of APT (if we consider a specific radius) or of MAPT/JMAPT (if we want to search for all radial symmetries in a specific range). A simple salient point detector can be realized with the following procedure: computation of the MAPT with evenly sampled radii R_n (with a sampling step sufficiently dense compared to σ_0); Gaussian smoothing; selection of local maxima of the 4-dimensional function with intensity higher than a chosen threshold. Note that this threshold has a well-defined meaning: we know that the expected value for a perfect sphere is 1, independently of the scale. We can choose the threshold as the value t corresponding to the fraction of an approximately spherical surface part that we want to detect in the specific application.

Salient points can be characterized with vector descriptors, including, for example, intensity and scale. Further descriptor components can be, for example, blobness, flatness and vesselness of the map in a neighborhood of the point that can be estimated from the eigenvalues of the inertia matrix.

We implemented this salient points detector and tested it on different shapes. The program computes from the input surface a reference length s equal to a fixed fraction of the square root of the total surface area $\sqrt{A_{tot}/80\pi}$. It then uses this value as minimum radius R_0, as step between the tested radii and as voxel dimension in the MAPT computation. The kernel size used at the different scales is given by $\sigma_i = 0.5R_i$. The threshold used to consider the detected local maxima salient points is 0.2.

Figure 18: Examples of salient points detected on models of animals and humans. They are represented as spheres with radius equal to half the detected scale and color encoding intensity (brightness) and sphericity (red component).

On non-perfectly symmetrical objects, salient points are still detected due to the tolerance given by s and their sphericity values characterize regions around differently shaped surfaces. Figure 18 shows results obtained on meshes representing animals and humans (from the SHREC 2011 nonrigid 3D watertight data), where the extracted salient points correspond to relevant anatomical features that are detected almost independently on pose. Figure 19 shows results obtained on three models of a girl acquired with a commercial whole body scanner device. Salient points corresponding to major anthropometric locations are detected and are rather similar in different poses even if the quality of the models is low and large holes and noise are present. We tested also salient points extraction as maxima of the 3D JMAPT: results are rather similar to those obtained on the 4D map, only the characterization with the inertia tensor is less reliable due to the mixture of signals at different scales.

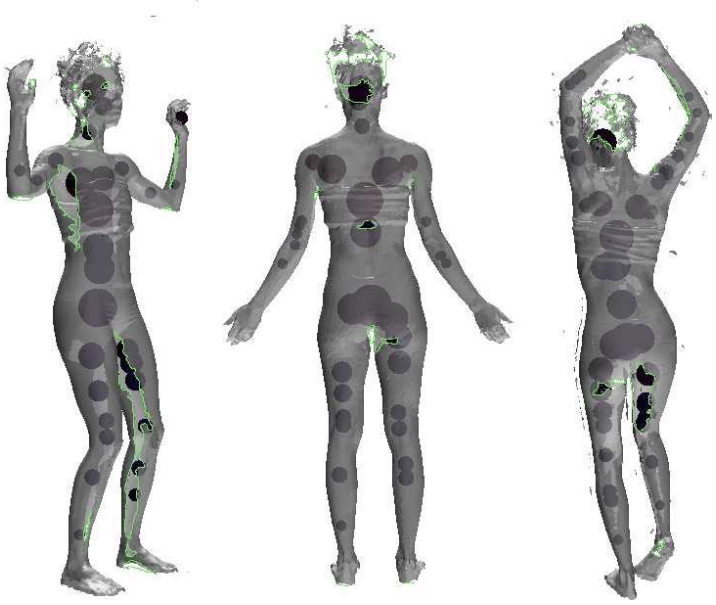

Figure 19: Salient points are reasonably extracted also in largely incomplete and noisy meshes as those here (large holes on visible sides highlighted in green), acquired with a whole body scanner on a subject in varying poses. Only maxima larger than a threshold (t = 0.2) are shown.

Lines extraction

Tubular parts of a shape should be characterized by a region of MAPT or JMAPT with high values, but also high vesselness with continuous orientation. Local vesselness and direction can be obtained in several ways analyzing local structure of the map or using area projection directional information.

We plan to perform further investigations in order to define the best APT-based skeletonization algorithm, meanwhile we used a method commonly applied in medical images for vascular segmentation based on Frangi's hessianbased vesselness estimation [64]. Local Hessian at the selected scale is also able to provide vessels direction and lines can be obtained tracking lines of maximal vesselness in the direction of the local vessel. To simply test the feasibility of the centerline extraction based on APT, we implemented the following simple procedure to compute skeletal paths:

- compute the multiscale vesselness map from the JMAPT;

- segment connected regions of non-negligible vesselness and continuous direction;
- find maxima of the map in each region and select points with the maximum distance from this point in opposite directions
- find the shortest path joining these points using fast marching with vesselness dependent speed.

This simple procedure provided visually reasonable results in tubular parts of the tested shapes. The algorithm does not provide connected paths as other methods (it is possible, however, to design specific heuristics to obtain such paths if needed). The method has, however, other interesting properties: it follows approximately tubular parts independently on local topology; in fact lines extracted do not correspond to centerlines of connected components, but to centerlines of cylindrical parts, so that, for example thumb skeleton is continued within the hand model in Figure 20 A. This can be a relevant advantage for applications, as shown in Figure 20 B.

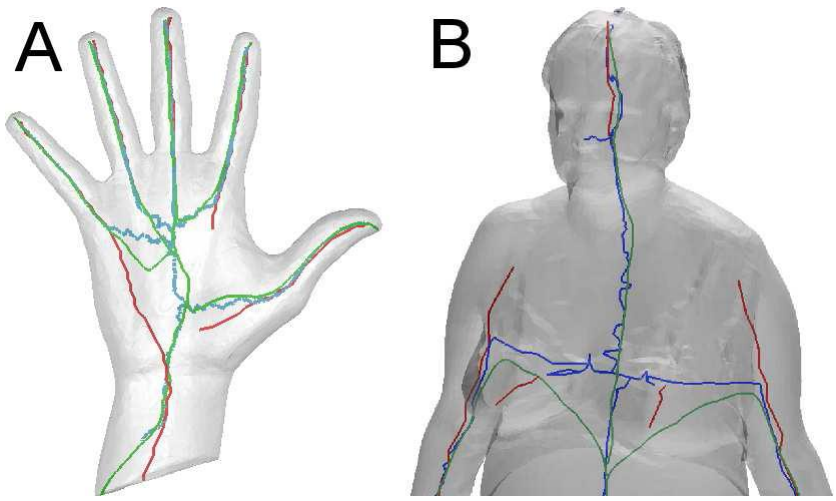

Figure 20: Lines extracted from the JMAPT are robust against topological noise. A: Skeletonization of a hand model. B: Lines extracted on a human body scan. Arms of the overweight woman are partially attached to the body. Curve skeleton algorithms often fail to follow the arms centerlines as in the case of publicly available codes based on medial geodesic function (blue) and voxel coding (green). Lines extracted with the APT method (red) follow the complete structures.

Most skeletonization methods commonly used fail to follow tubular parts partially attached on one side (as required for correct anthropometric evaluation), as it happens, for example in the case of limbs in scanned human bodies. Lines extracted with publicly available implementations of methods based on medial geodesic function [44] and voxel coding [57] do not follow the complete arm centerline, but the APT based method does. Furthermore, the method works on non-watertight surfaces and it is robust against the presence of relevant holes. We show this in the examples of Figure 21 where many of the lines extracted are not changed even if a relevant percentage of the meshes triangles are removed.

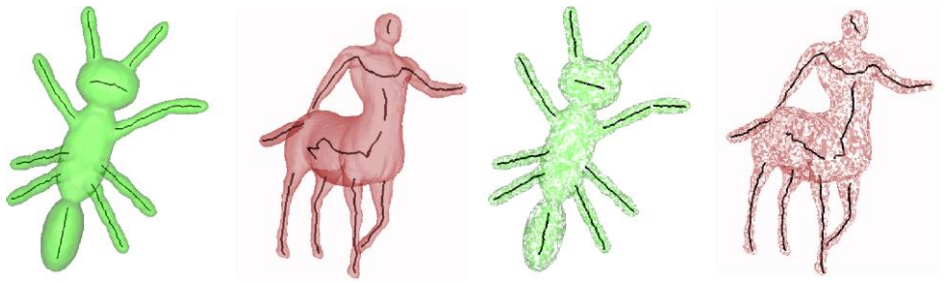

Figure 21: Lines extracted with the JMAPT method are robust against random triangle removal. Left: lines extracted on two models from the SHREC 2011 database. Right: lines extracted from the same models removing 50% of the original faces.

Points matching and semantic labeling through Radial Symmetry Graphs

CASS points computed on models differing for an articulated deformation almost stable and are rather similar in object of the same types (e.g. humans, animals). We can therefore try to match them, and even if the local characterization is poor, we can exploit for the task descriptors based on the similarity of paths starting from each point (e.g. average/median path distances, histograms of paths length or paths features) to characterize them with a robust contextual information. We plan to test several descriptors of this kind as future work.

In the meanwhile we implemented a simple "counting" procedure to match corresponding points of two graphs extracted on similar objects. Given a new graph and a template one we perform the following steps:

- initialize a counter for each label at each point
- for each path of the new model search for the nearest neighbor among the paths extracted on the template and increment the counters of the extremal points corresponding to the labels of the corresponding points of the closer path of the template.
- select as the best match the point with the maximally valued counter

A problem of this procedure is that it cannot distinguish between symmetric parts creating points with similar paths. We can, however, modify the procedure performing just a semantic labeling of the point set, using in the procedure non unique labels for the template points identifying simply a point type (e.g. leg, back, head, ear, etc).

Figure 22 shows examples of CASS salient points and corresponding "cleaned" symmetry graphs. It is possible to see that they resemble curve skeletons in tubular parts, but characterize also the other parts linking salient points and their computation is robust against noise and holes.

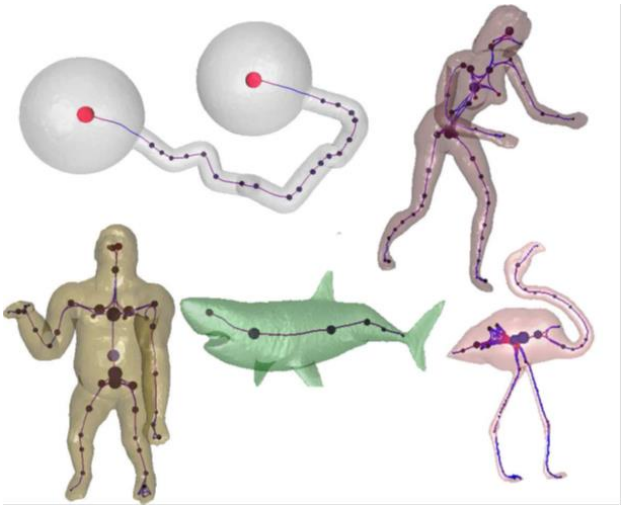

Figure 22: Examples of cleaned Radial Symmetry Graphs computed on different shapes.

A limit in the possibility of using points and paths for matching is surely related to the fact that in articulated shapes points can be created by (see the shark in Figure 3). Most of the points are, in any case stable in different poses, as shown in Figure 23.

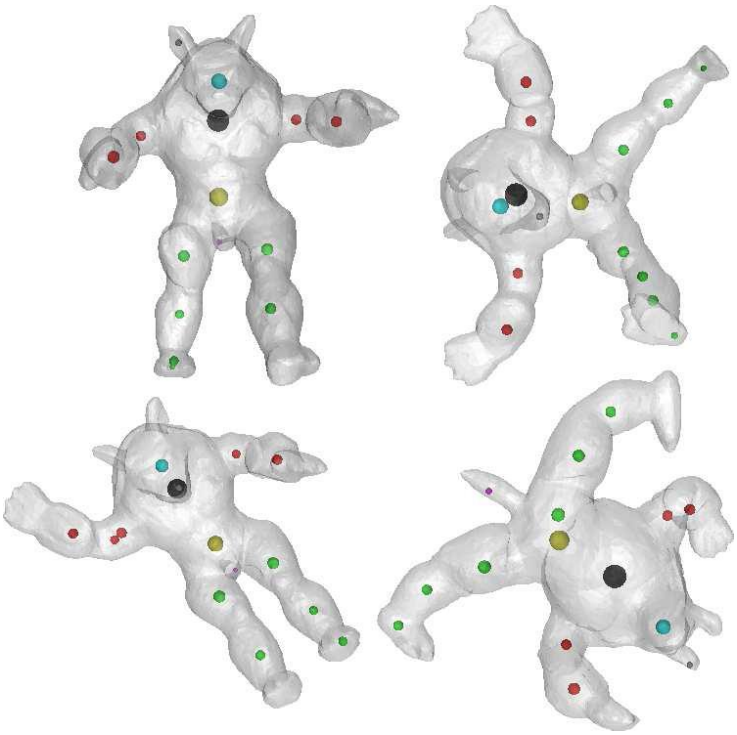

Figure 23: Automatic labelling of the highest valued 15 CASS points for armadillos in different poses obtained from a single manually labelled template.

We tested the semantic labelling obtained with the simple "voting" procedure on a set of models from the SHREC 2011 nonrigid watertight dataset [65]. Labelling a the salient points of the template model of an armadillo as head, trunk, back, arms, legs, nose, ear, chest, pelvis we were able to assign the right labels to more than 90% of the 15 CASS points of other 10 models deformed through an articulated transform (Figure 23) using the labels manually given to a single template (pose of Figure 13) as example.

4. Discussion

We discuss separately the results of two anthropometric experiments and of area projection transform.

Experiment 1

Validation of the Breuckmann body Scanner for anthropometry

Body scanners are increasingly used in health assessment and physical anthropology [48,49,50,66] and it is probable that they will represent the standard anthropometric tool in the future. In this work we evaluated the ability of a 3D scanner, the Breuckmann BodySCAN, to allow reliable anthropometric measurements.

Results show that when duplicate measurements are performed of standard anthropometric parameters by and experienced anthropometrist, excellent correlation coefficient r is found in either the manual or digital mode; this suggests that digital measurement of anthropometric parameters is at least as reliable as manual. In order to check for possible systematic error in measurement the t test was also performed, showing significant/borderline difference of the duplicate means in four and none anthropometric parameters with the manual and digital mode, respectively. This suggests that digital measurements are less prone to systematic measurement error. The ICC, an alternative test of reliability using the F test from repeated measures analysis of variance, was high (>0.9) for all measurements in the manual mode; in the digital mode, the ICC was somewhat lower for some anthropometric parameters, still

showing high P values. This indicates that digital measurement is at least comparable to manual in terms of reproducibility.

When the agreement of manual and digital measurements taken by the experienced anthropometrist was tested, the ICC resulted good (>0.8-<0.9) to high (>0.9) in the majority of anthropometric parameters. As expected, less than satisfactory agreement was found for head circumference due to the better performance of manual measurement in minimizing hair bias; further investigation is needed to clarify the reason for the relative disagreement in wrist and bi-epicondilar measurements.

Interestingly, when naïve anthropometrists took measurements in the digital mode the correlation coefficient r and the ICC for duplicate measurements were mostly high (>0.9) with no systematic error (as assessed by t test); this clearly show that digital anthropometry, which is independent of subject's movement/sway as well as most ambient detrimental factors e.g., noise, temperature or observer-subject interaction allows for good to excellent measurement performance of observers in the absence of specific time-consuming training.

In conclusion, the Breuckmann BodySCAN revealed a reliable and effective tool for digital anthropometry comparing well with traditional manual procedures as well as allowing for reproducible measurements in the absence of specific anthropometric training.

Experiment 2

Health-related shape analysis of 3D Scanner Data

We evaluated the ability of completely automatic measurements performed on body scanner data to predict body fat in obese female subjects. The results obtained suggest that some of the tested measurements can predict subtotal body fat similarly to standard anthropometric

measurements, while they seem to correlate even better than tape-based anthropometric parameters with trunk fat. The high correlation of the maxima of mean diameter and section area with subtotal fat is not trivial, and the fact that simple measures on the trunk region are correlated with a whole body parameter, not easily estimated by other means deserves further investigation.

An interesting outcome of our analysis is that automatically computed measurements seem to be more correlated with trunk fat than similar parameters measured with the tape-based method. This could be due to the difficulty to locate precisely the landmarks on obese subjects and perhaps the possibly large deformations on the soft tissue created by the tape and calipers during the measurement process. This means that, even if the automatic measurement system is limited by several factors due to acquisition protocols and processing algorithm, indexes evaluated from the automatic system may be more effective than those coming from manual measurements (and, clearly, they are computed faster and with no user intervention).

We plan, however, to improve the accuracy of the automatic system and perform several validation tests on them, trying to solve problems that are not well treated by our current methods. A source of errors that make some parameters to lose precision, for example, is the pose of the arms of the subjects, which make latero-lateral measurements difficult where the arm adhered to lateral trunk surface. Moreover, in obese subjects the shape of the abdomen region is dependent on the underwear worn during the acquisition. This can introduce some errors on measurements localized in this region.

Experiment 3

Area projection transform

We developed a novel method for detecting radial symmetries of 3D shapes by computing a spatial function called multiscale area projection transform, defined for generic surfaces and

implemented for triangulated meshes. We have shown its possible use for relevant tasks such as salient points detection and centerline tracking. The results obtained in a complex shape retrieval task with our method based on MAPT histograms revealed its ability to capture both global and local object features and are particularly remarkable considering that method is scale invariant, can be applied also to non-watertight meshes, it is robust against topological noise and could be used as well on dense point clouds instead of meshes, projecting points along associated normal and assuming that their density is approximately constant.

Moreover, we proposed a new robust characterization of shapes based on the extraction of salient points (CASS) computed from the Joint Multiscale Area Projection Transform and the creation of a graph (Radial Simmetry Graph) obtained by joining these points following maximal JMAPT paths. This shape characterization inherits the robustness against noise, holes and topological changes of the original transform. The graph structure can be useful for matching purposes adding contextual information to the point characterization and could also be applied to intrinsic symmetry detection. In a first test we were able to assign a semantic label to salient points of articulated objects in different poses from a labelled example, using a simple path distance based voting.

Conclusions

Anthropometry performed through body scanner devices is spreading, resulting in a deep change in the way anthropometric analyses are performed. This leads to simpler and faster anthropometric procedures. This technology finds new applications every day and there is still much to do to exploit it potentials in healthcare.

In my opinion one of the major obstacles to the full employing of the technology come from the lack of scientific knowledge we have about the connections of so called “body shape” and the material living substrate from which the first derive. While the “first layer” of body shape determinants i.e. the muscolo-skleletal system and the body fat are object of active research, scanner technology is suitable to systematically investigate more subtle but interesting connection, e.g with psychology (exploiting the relationship between posture and emotions) and epigenetics, as exemplified in [67].

Moreover, while 3D shape analysis hasn’t yet defined standardized methods that can cope with all *desiderata* of anthropometry (and, in general, of morphometry applied to biology) there is still a lot of research to perform to fill the gap. My experience lead me to consider that the field of computer science and biological/medical science can positively stimulate each other, the first with innovative investigation instruments, the second with challenging tasks.

I further observe that, in order to obtain substantial results, this genre of research has necessarily to be conducted by multidisciplinary teams, where a hybrid form of knowledge can be shared. The different “philosophies” historically implied in different branch of scientific knowledge results in communication barriers, a general frame in which such a type of common knowledge can be shared could be necessary. Good candidates for this role can be the general theory of systems of Von Bertalannfy [68] and the epistemology of complexity [69]

References

1. Norton, K.,Olds, T., (Eds), (2001): “Anthropometrica: A Textbook Of Body Measurement For Sports And Health Courses”, University Of New South Wales Press.

2. Kouchi M, Mochimaru M, Tsuzuki K, Yokoi T., (1999): “Interobserver errors in anthropometry”, Journal of Human Ergology (Tokyo)” Vol. 28, pp15-24.

3. Bubb, H., (2004): “Challenges in the application of anthropometric measurements”, Theoretical Issues in Ergonomic Science Vol.5, No 2, pp.154-168.

4. Robinette, K.M., Daanen, H.A., (2006): “Precision of the CAESAR scan-extracted measurements”, Applied Ergonomics. Vol.37, No.3, pp.259-265.

5. Cyberware inc. web site (accessed 2010): http://www.cyberware.com.

6. Hamamatsu photonics web site (accessed 2010): http://www.hamamatsu.com.

7. Vitronic inc. web site (accessed 2010): http://www.vitronic.de.

8. Human solutions web site (accessed 2010): http://www.human-solutions.com

9. Visualization toolkit web site (accessed 2010): http://www.vtk.org.

10. Textile and clothing technology corporation web site (accessed 2010): http://www.tc2.com

11. Inspeck inc. web site (accessed 2010): http://www.inspeck.com

12. Breuckmann gmbh web site (accessed 2010): http://www.breuckmann.com.

13. Bray GA, Bellanger T. Epidemiology, trends, and morbidities of obesity and the metabolic syndrome. Endocrine 2006; 29:109–117.

14. Mokdad AH, Ford ES, Bowman BA, Dietz WH, Vinicor F, Bales VS et al. Prevalence of obesity, diabetes, and obesity-related health risk factors, 2001. JAMA 2003; 289: 76–79.

15. McTiernan A. Obesity and cancer: the risks, science, and potential management strategies. Oncology 2005; 19: 871–881.

16. Canoy D, Luben R, Welch A, Bingham S, Wareham N, Day N et al. Abdominal obesity and respiratory function in men and women in the EPIC-Norfolk Study, United Kingdom. Am J Epidemiol 2004; 159: 1140–1149.

17. Garlie, T. N., Obusek, J. P., Corner, B. D. and Zambraski, E. J. (2010), Comparison of body fat estimates using 3D digital laser scans, direct manual anthropometry, and DXA in men. Am. J. Hum. Biol., 22: 695–701.

18. R. Pargas. Automatic measurement extraction for apparel from a three- dimensional body scan. Optics and Lasers in Engineering, 28:157{172, September 1997.

19. Karia P. Simmons. Body measurement techniques: a comparison of three- dimensional scanning and physical anthropometric methods. Ph.D dissertation, North Carolina State University, 2001.

20. Zouhour Ben Azouz, Chang Shu, and Anja Mantel. Automatic locating of anthropometric landmarks on 3d human models. In 3DPVT '06: Proceedings of the Third International Symposium on 3D Data Processing, Visualization, and Transmission (3DPVT'06), pages 750-757, Washington, DC, USA, 2006. IEEE Computer Society.

21. Iat-Fai Leong, Jing-Jing Fang, and Ming-June Tsai. Automatic body feature extraction from a marker-less scanned human body. Comput. Aided Des., 39(7):568-582, 2007.

22. Werghi, N.: Segmentation and modeling of full human body shape from 3-d scan data: A survey. IEEE Transactions on Systems, Man, and Cybernetics, Part C 37(6), 1122–1136 (2007)

23. Xiao, Y., Siebert, P., Werghi, N.: A discrete reeb graph approach for the segmentation of human body scans. In: Proceedings of Fourth International Conference on3-D Digital Imaging and Modeling, 2003. 3DIM 2003, pp. 378–385 (2003)

24. Werghi, N.: A robust approach for constructing a graph representation of articulated and tubular-like objects from 3d scattered data. Pattern Recognition Letters 27, 643–651 (2007)

25. Mortara, M., Patané, G., Spagnuolo, M.: From geometric to semantic human body models. Computers & Graphics, 185–196 (2006)

26. Yu, Y., Wang, Z., Xia, S., Mao, T.: Automatic joints extraction of scanned human body. HCI (12), 286–293 (2007)

27. Lee C., Varshney A., Jacobs D.: Mesh saliency. ACM Trans. Graph. 24 (July 2005), 659–666.

28. Shilane P., Funkouser T.: Selecting distinctive 3D shape descriptors for similarity retrieval. In International Conference on Shape Modelling and Applications (2006), IEEE Computer Society, p. 18.

29. Castellani U., Cristani M., Fantoni S., Murino V.: Sparse points matching by combining 3D mesh saliency with statistical descriptors. Computer Graphics Forum27 (2008), 643–652.

30. Johnson A., Herbert M.: Using spin images for efficient object recognition in cluttered 3d scenes. IEEE Transactions on Pattern Analysis and Machine Intelligence 21, 1 (May 1999), 433 – 449.

31. Maes C., Fabry T., Keustermans J., Smeets D., Suetens P., Vandermeulen D.: Feature detection on 3d face surfaces for pose normalisation and recogntiion. In BTAS ’10, IEEE Int. Conf. on Biometrics: Theory, Applications and Systems (2010), pp. 1–6.

32. Körtgen M., Park G., Novotni M., Klein R.: 3d shape matching with 3d shape contexts. In The 7th Central European Seminar on Computer Graphics (Apr. 2003).

33. Bronstein A. M., Bronstein M. M., Castellani U., Falcidieno B., Fusiello A., Godil A., Guibas L. J., Kokkinos I., Lian Z., Ovsjanikov M., Patane G., Spagnuolo M., Toldo R.: Shrec 2010: robust large-scale shape retrieval benchmark. In Proc. EUROGRAPHICS Workshop on 3D Object Retrieval (2010).

34. Lian Z., Godil A., Bustos B., Daoudi M., Hermans J., Kawamura S., Kurita Y., Lavoué G., Nguyen H., Ohbuchi R., Ohkita Y., Ohishi Y., Porikli F., Reuter M., Sipiran I., Smeets D., Suetens P., Tabia H., Vandermeulen D.: Shrec'11 track: Shape retrieval on non-rigid 3d watertight meshes. In Proc. Eurographics/ACM SIG-GRAPH Symposium on 3D Object Retrieval (2011), pp. 79–88.

35. Cornea N. D., Silver D., Min P.: Curve-skeleton properties, applications, and algorithms. IEEE Transactions on Visualization and Computer Graphics 13, 3 (2007), 530–548.

36. Blum H.: A Transformation for Extracting New Descriptors of Shape. In Models for the Perception of Speech and Visual Form, Wathen-Dunn W., (Ed.). MIT Press, Cambridge , 1967, pp. 362–380.

37. Sundar H., Silver D., Gagvani N., Dickinson S.: Skeleton based shape matching and retrieval. In Proc. Shape Modeling International (Washington , DC , USA , 2003), IEEE Computer Society, p. 130.

38. Cornea, N., Silver, D., Yuan, X., Balasubramanian, R.: Curve-skeleton applications. In: IEEE Visualization, pp. 95–102 (2005).

39. Gagvani, N., Silver, D.: Parameter-controlled volume thinning. Graph. Models and Image Proc. (3), 149–164 (1999).

40. Shapira, L., Shamir, A., Cohen-Or, D.: Consistent mesh partitioning and skeletonization using the shape diameter function. Vis. Comput. 24(4), 249–259 (2008)

41. van Wijk, J.J., Telea, A.: An augmented fast. marching method for computing skeletons and centerlines. In: Proc. IEEE VisSym 2002, pp. 251–260. ACM Press, New York (2002)

42. Cornea, N., Silver, D., Yuan, X., Balasubramanian, R.: Computing hierarchical curve-skeleton of 3d objects. The Visual Computer (11), 945–955 (2005)

43. Sharf, A., Lewiner, T., Shamir, A., Kobbelt, L.: On-the-fly curve-skeleton computation for 3d shapes. The Visual Computer 26(3) (2007)

44. Dey, T.K., Sun, J.: Defining and computing curve-skeletons with medial geodesic function. In: SGP 2006: Proceedings of the fourth Eurographics symposium on Geometry processing, Aire-la-Ville, Switzerland, pp. 143–152. Eurographics Association (2006)

45. Reniers, D., Van Wijk, J.J., Telea, A.: Computing multiscale curve and surface skeletons of genus 0 shapes using a global importance measure. IEEE Transactions on Visualization and Computer Graphics 14(2), 355–368 (2008).

46. SizeUK on Sizemic website (accessed march 2013): http://www.sizemic.eu/sizeuk.html

47. SizeUSA web site (accessed march 2013): http://www.sizeusa.com

48. Wang J, Gallagher D, Thornton JC, Yu W, Horlick M, and Pi-Sunyer FX. Validation of a 3-dimensional photonic scanner for the measurement of body volumes, dimensions and percentage body fat. Am J Clin Nutr, pages 809-816, 2006.

49. Wells JC, Cole TJ, Bruner D, and Treleaven P. Body shape in American and British adults: between-country and inter-ethnic comparisons. Int J Obes., pages 152–159

50. Lin JD, Chiou WK, Weng HF, Fang JT, and Liu TH. Application of three-dimensional body scanner: observation of prevalence of metabolic syndrome. Clin Nutr., pages 1313–23, 2004

51. Visualization Toolkit website (acc. march 2013) http://www.vtk.org

52. Qt project website (acc. march 2013) http://qt-project.org/

53. Lohman, T.G., Roche, A.F., Martorell, R. (eds.), (1988): "Anthropometric Standardization Reference Manual", Human Kinetics Books, Champaign Ill.

54. Lovato, C., Castellani, U., Fantoni, S., Milanese, C., Zancanaro, C. Giachetti, A. (2009): "Computer assisted estimation of anthropometric parameters from whole body scanner data", 2nd Workshop on 3D Physiological Human, LNCS 5903, pp71-83.

55. Andreoli A., Scalzo G. et al. (2009) "Body composition assessment by dual-energy X-ray absorptiometry (DXA)", La Radiologia Medica, 2009 114:286-300

56. Cignoni P., Callieri M., Corsini M.et al. "MeshLab: an Open-Source Mesh Processing Tool", Proceedings of Eurographics Italian Chapter Conference 2008: 129-136

57. Lovato C., Castellani U., Giachetti A. (2009) "Automatic Segmentation of Scanned Human Body Using Curve Skeleton Analysis". MIRAGE 2009:34-45

58. Wintner A.: On parallel surfaces. American Journal of Mathematics 74, 2 (1952), 365–376.

59. Chazal F., Lieutier A.: The "λ-medial axis". Graph. Models 67, 4 (July 2005), 304–331.

60. Miklos B., Giesen J., Pauly M.: Discrete scale axis representations for 3d geometry. ACM Transactions on Graphics (TOG) 29, 4 (2010), 101.

61. Deschamps T.; Cohen L.D. et al.: Fast extraction of minimal paths in 3d images and applications to virtual endoscopy. Medical Image Analysis 5, 4 (2001), 281–299.

62. Giachetti A., Lovato C.: Radial symmetry detection and shape characterization with the multiscale area projection transform. Comp. Graph. Forum 31, 5 (Aug. 2012), 1669–1678.

63. Bai X., Latecki L.: Path similarity skeleton graph matching. Pattern Analysis and Machine Intelligence, IEEE Transactions on 30, 7 (july 2008), 1282 –1292.

64. Frangi A., Niessen W., Vincken K., Viergever M.: Multiscale vessel enhancement filtering. In Medical Image Computing and Computer-Assisted Interventation-MICCAI'98, Wells W., Colchester A., Delp S., (Eds.), vol. 1496 of Lecture Notes in Computer Science. Springer Berlin / Heidelberg , 1998, pp. 130–137.

65. Lianz Z., Godil A., Bustos B., Daoudi M. et al.: Shrec'11 track: Shape retrieval on non-rigid 3d watertight meshes. In Proc. Eurographics/ACM SIGGRAPH Symposium on 3D Object Retrieval (2011), pp. 79–88.

66. Wells, J.C., Cole, T.J., Treleaven , P. (2008): "Age-variability in body shape associated with excess weight: the UK national sizing survey", Obesity, Vol.16, No.2, pp.435-441.

67. Chinthapalli K, Bartolini E, Novy J, Suttie M, Marini C, Falchi M, Fox Z, Clayton LM, Sander JW, Guerrini R, Depondt C, Hennekam R, Hammond P, Sisodiya SM. Atypical face shape and genomic structural variants in epilepsy. Brain. 2012 Oct;135(Pt 10):3101-14.

68. Ludwig von Bertalanffy, 1968, General System Theory. Development, Applications, George Braziller, New York, trad. it. Teoria Generale dei Sistemi, Oscar Saggi Mondadori, 2004.

69. Edgar Morin, 1990 Introduction à la pensèe complexe, Seuil, Paris trad. It. Introduzione al pensiero complesso, Sperling & Kupfer, Milano, 1993